18-435.R1 Poulsom Edited USA English ORIGINAL PAPER

Neutrophil elastase plays a non-redundant role in remodeling the venular basement membrane and neutrophil diapedesis post ischemia/reperfusion injury

Mathieu-Benoit Voisin [1*], Giovanna Leoni [1,2], Abigail Woodfin [1], Laure Loumagne [1], Nimesh S. A. Patel [1], Rosanna Di Paola [3], Salvatore Cuzzocrea [3], Christoph Thiemermann [1], Mauro Perretti [1] and Sussan Nourshargh [1].

[1] William Harvey Research Institute, Barts and The London School of Medicine and Dentistry, Queen Mary University of London, UK; [2] Institute for Cardiovascular Prevention (IPEK), Ludwig-Maximilian University (LMU), Munich, Germany; [3] Department of Chemical, Biological, Pharmaceutical and Environmental Sciences, University of Messina, Messina, Italy.

**Correspondence to: Mathieu-Benoit Voisin, William Harvey Research Institute, Barts & The London School of Medicine and Dentistry, Queen Mary University of London, Charterhouse Square, London, EC1M 6BQ, UK. E-mail: m.b.voisin@qmul.ac.uk*

Short Running title: NE mediates neutrophil breaching of venular basement membrane in I/R injury

The authors declare that there is no conflict of interest to disclose.

Word count: 4,665 (OK)

ABSTRACT

Ischemia/reperfusion (I/R) injury is a severe inflammatory insult associated with numerous pathologies such as myocardial infarction, stroke and acute kidney injury. I/R injury is characterized by a rapid influx of activated neutrophils secreting toxic free radical species and degrading enzymes that can irreversibly damage the tissue, thus impairing organ functions. Significant efforts have been invested in identifying therapeutic targets to suppress neutrophil recruitment and activation post I/R injury. In this context, pharmacological targeting of neutrophil elastase (NE) has shown promising anti-inflammatory efficacy in a number of experimental and clinical settings of I/R injury, and is considered a plausible clinical strategy for organ care. However, the mechanisms of action of NE, and hence its inhibitors, in this process is not fully understood. Here we conducted a comprehensive analysis of the impact of NE genetic deletion on neutrophil infiltration in four murine models of I/R injury as induced in the heart, kidneys, intestine and cremaster muscle. In all models, neutrophil migration into ischemic regions was significantly suppressed in $NE^{-/-}$ mice as compared to wild-type controls. Analysis of inflamed cremaster muscle and mesenteric microvessels by intravital and confocal microscopy revealed a selective entrapment of neutrophils within venular walls, most notably at the level of the venular basement membrane (BM) following NE-deletion/pharmacological blockade. This effect was associated with the suppression of NE-mediated remodeling of the low matrix protein expressing regions within the venular BM used by transmigrating neutrophils as exit portals. Furthermore, whilst NE deficiency led to reduced neutrophil activation and vascular leakage, levels of monocytes and pro-healing M2 macrophages were reduced in tissues of $NE^{-/-}$ mice subjected to I/R. Collectively our results identify a vital and non-redundant role for NE in supporting neutrophil breaching of the venular BM post I/R injury but also suggest a protective role for NE in promoting tissue repair.

Key words:

Neutrophil, Elastase, Ischemia/Reperfusion Injury, Venular Basement Membrane

INTRODUCTION

Ischemia/reperfusion (I/R) injury is a common feature of many cardiovascular pathologies such as myocardial infarction, cerebral stroke and clinical complications associated with organ transplantation surgeries [1-4]. The occurrence of I/R injury is paradoxical in that it is induced following the often life-saving process of restoration of blood flow to ischemic tissues. Whilst this practice is aimed at providing nutrients and oxygen to affected regions, and hence preventing tissue necrosis, the procedure can lead to vascular dysfunction [5], acute inflammation and ultimately increase in tissue-cell death [6]. This pathophysiological response is largely the consequence of a rapid activation of the vascular endothelium and an intense recruitment of pro-inflammatory leukocytes [7].

Neutrophils are the first leukocytes to be recruited to sites of I/R injury. These innate immune cells, whilst vital for host defense against pathogens are implicated in the pathogenesis of many disorders due to their capacity to release a wide range of pro-inflammatory mediators [8,9], reactive oxygen species [10] and destructive proteolytic enzymes. Clear evidence for the involvement of neutrophils in I/R injury has been provided by both preclinical and clinical studies in which neutrophil depletion was protective against further tissue damage [11-14]. Similarly, blocking neutrophil interaction with blood vessel walls within reperfused areas of ischemic tissues improves disease outcome in patients [15-17]. However, the inhibitors used in such settings are not solely specific for neutrophil recruitment and also blocked the migration of other leukocyte sub-types, including monocytes that can contribute to tissue healing. As such, there remains a need for alternative therapeutic approaches for suppressing neutrophil migration and their destructive potential following I/R injury.

Neutrophil Elastase (NE) is the most abundant protease expressed by neutrophils [18,19] and that is rapidly released from azurophilic granules upon activation. This serine protease can act on a broad range of substrates including extracellular matrix components, pro-enzymes, adhesion molecules, signaling receptors and cytokines [20,21]. It also has strong antibacterial properties and is implicated in NETosis [22]. Due to this wide-ranging substrate specificity and function, NE has been implicated in numerous physiological and pathological scenarios including I/R injury [23]; and is considered as a good indicator of disease severity in respiratory and cardiovascular pathologies [24,25]. Interestingly, natural and synthetic NE blockers inhibit I/R-induced inflammation in both pre-clinical and clinical studies [26]. In sharp contrast, NE-deficient animals ($NE^{-/-}$) showed normal neutrophil recruitment in experimental models of cytokine-induced inflammation [27] and bacterial infection [28,29]. Taken together, such conflicting studies suggest a stimulus-specific role for NE as a regulator of neutrophil trafficking, and importantly highlight the lack of understanding of the mechanisms through which NE regulates neutrophil migration and possibly activation.

The aim of the present study was to re-evaluate the potential strength of NE as a therapeutic target for suppression of I/R-induced inflammation and to ascertain its mechanism of action in mediating neutrophil trafficking post I/R injury. We hypothesized that during I/R injury, NE is rapidly induced on the cell surface of transmigrating neutrophils, and as such plays a unique and non-redundant role in facilitating neutrophil migration through blood venular walls. For this purpose, we investigated the role of NE using both NE-deficient mice and a well-characterized NE inhibitor (ONO-5046, sivelestat) [30], in multiple disease-mimicking murine models of I/R injury, including models of myocardial and renal I/R injury; and have ascertained the site of arrest of neutrophils at

the level of the venular basement membrane under conditions of NE deletion/blockade during I/R injury. Mechanistically, the function of NE was linked to its mobilization from transmigrating neutrophils within the venular basement membrane (BM) and its ability to remodel neutrophil permissive regions within the venular BM termed low expression regions (LERs). Overall, the present findings provide unequivocal evidence for an essential role for NE in neutrophil migration through venular walls in I/R injury, identifying the breaching of the venular BM as a key NE-mediated stage of neutrophil trafficking during this pathology.

MATERIALS AND METHODS

Detailed materials and methods are available in supplementary material, Supplementary Materials and methods.

Animals

NE knock-out ($NE^{-/-}$) male mice and C57BL/6 wild-type (WT) animals were employed. All animal experiments were conducted in accordance with the United Kingdom Home Office legislation and NC3R recommendations.

Treatments

Anaesthetized WT mice were injected via jugular vein cannulation with saline or with sivelestat (ONO-5046) with an initial dose of 50 mg/kg in a 200 µl bolus followed by an infusion of 50 mg/kg at 200 µl per hour.

Ischemia/reperfusion injury of the heart:

Anaesthetized animals were subjected to myocardial infarction by ligation of the left anterior descending coronary artery for 25 min, followed by a reperfusion period of 2 h.

Ischemia/reperfusion injury of the kidneys:

Anaesthetized animals were subjected to bilateral renal ischemia for 30 min followed by a 24 h reperfusion period.

Intravital microscopy and induction of cremasteric ischemia/reperfusion injury

The cremaster muscle was surgically exteriorized and subjected to ischemia using an artery clamp placed at the proximal end of the cremaster tissue for 30 min. Blood flow was then restored by releasing the clamp and reperfusion was allowed to develop for up to 2 h. Leukocyte responses (adhesion and extravasation) were observed on an upright bright-field microscope.

Intravital microscopy and induction of ischemia/reperfusion injury of the mesenteric tissue

Mesenteric ischemia was induced by clamping the superior mesenteric artery for 35 min before allowing the reperfusion of the tissue for 90 min. Leukocyte responses (adhesion and extravasation) were quantified within mesenteric post-capillary venules.

Determination of renal injury and dysfunction

Histological evaluation was performed on kidney sections stained with hematoxylin and eosin, and viewed using a bright-field microscope. The serum levels of creatinine and aspartate aminotransferase were quantified by ELISA.

Adoptive cell transfer experiments

Bone marrow leukocytes from WT or $NE^{-/-}$ donor mice were fluorescently labeled with PKH26 according to the manufacturer's recommendations and injected intravenously into WT or $NE^{-/-}$ recipient animals via the tail vein prior to I/R injury of the cremaster muscles as detailed above. At the end of the reperfusion period, the harvested tissues were immunostained for confocal microscopy analysis. Blood samples were also taken by cardiac puncture, and the number of circulating PKH26+ cells was analyzed by flow cytometry.

Analysis of tissues by immunofluorescence labeling and confocal microscopy:

Detection of neutrophils into the ischemic region of the heart was performed on OCT-embedded heart tissue sections immunostained for collagen IV, endothelial cells and neutrophils. For localization of neutrophils into the cremaster muscles and mesenteric tissue following I/R injury, whole-mount tissues were fluorescently immunostained for neutrophils, the endothelium and the perivascular BM. For NE expression, tissues were fluorescently immunostained for neutrophils, NE and the perivascular BM. For NE activity, the NE-fluorescent activatable substrate NE680FAST (Perkin Elmer, Beaconsfield, UK) was injected i.v. prior to reperfusion. All samples were viewed using laser-scanning confocal microscopes and images were analyzed using IMARIS software. The area and intensity of matrix protein "Low expression regions" (LERs) within the perivascular basement membrane were measured using ImageJ (NIH & Laboratory for Optical and Computational Instrumentation, University of Wisconsin, USA).

Vascular leakage

Vascular leakage upon I/R injury was quantified using the Miles assay [31].

Flow cytometry analysis of leukocyte subpopulation

Leukocyte subpopulations (neutrophils, monocytes and macrophages) present in the cremaster muscles and their phenotype were assessed by flow cytometry 20 h post I/R injury.

Statistical analyses

All data were processed and analyzed using GraphPad Prism 6 software (GraphPad Inc, San Diego, CA, USA), and are presented as mean ± SEM. Statistical significance was assessed by parametric or non-parametric tests according to the sample size of the data analyzed. $P < 0.05$ taken as statistically significant.

RESULTS

NE-deficient mice exhibit reduced neutrophil infiltration in models of myocardial and kidney ischemia reperfusion injury

To ascertain the role of NE in neutrophil recruitment in clinically relevant models of I/R injury, we investigated the impact of genetic deletion of NE in murine models of myocardial and kidney I/R injury. With respect to the heart injury model, WT and $NE^{-/-}$ animals were subjected to myocardial infarction (MI) for 25 min followed by 2 h of reperfusion. The degree of tissue injury (depicted by increased anti-collagen mAb immunoreactivity) and levels of neutrophil infiltration into the heart ischemic region were investigated by confocal microscopy. WT mice subjected to MI exhibited an intense remodeling of the myocardial tissue, as illustrated by increased collagen-IV immunoreactivity in the ischemic area **(Figure 1A,B)**, a response that was associated with a significant infiltration of neutrophils specifically in this region **(Figure 1C)** as compared to sham-operated WT mice **(Figure 1D,E)**. In contrast, $NE^{-/-}$ animals subjected to MI exhibited a similar morphology and levels of collagen IV immune-reactivity to that seen in sham-operated animals **(Figure 1A,B)**. Interestingly, $NE^{-/-}$ mice exhibited no increase in local neutrophil infiltration post MI as compared to WT animals **(Figure 1D,E).**

To ascertain the generality of the protective effect of NE genetic deficiency against I/R injury and neutrophil infiltration, we next investigated a model of renal I/R injury. Here, mice were subjected to bi-lateral renal ischemia for 30 min followed by reperfusion for 24 h before collecting kidney and blood samples to assess the extent of local tissue damage, leukocyte infiltration and the loss of renal functions post I/R. Histological examination of WT kidneys subjected to I/R showed evidence of renal injury as exemplified by the

degeneration of proximal and distal tubules, tubular swelling and necrosis, and luminal congestion, as compared to sham-operated animals **(Figure 2A,B)**. This response was also associated with increased PMN infiltration **(Figure 2C, Supplementary material, Figure S1A)**. In contrast, $NE^{-/-}$ animals subjected to renal I/R showed almost normal kidney structure organization and an ~80% reduction in leukocyte infiltration**.** Analysis of sera from WT mice subjected to renal I/R showed a significant increase in markers of renal dysfunction/injury, namely high levels of creatinine and aspartate aminotransferase, as compared to levels detected in serum of both sham-operated WT mice and $NE^{-/-}$ animals subjected to kidney I/R **(Supplementary material, Figure 1B,C).**

Collectively these results demonstrate that NE deficiency is protective in both models of MI and renal I/R injury, an effect that involved a marked inhibition of the acute neutrophil recruitment to locally injured tissues.

NE deficiency inhibits I/R-induced neutrophil migration into tissues by selectively suppressing breaching of venular walls at the level of the basement membrane

To gain insight into the mechanism through which NE mediates I/R-induced neutrophil recruitment, we sought to determine the stage of the emigration cascade at which NE acts. For this purpose, we first applied intravital microscopy (IVM) to the analysis of leukocyte responses within cremasteric venules of WT and $NE^{-/-}$ mice subjected to local I/R injury, as previously described [32,33]. Within this I/R model, robust and time-dependent leukocyte adhesion and transmigration responses were noted within the 2 h reperfusion period in WT mice, as compared to sham-operated animals **(Figure 3A, Supplementary material, Movies S1, S2**). Interestingly, neutrophil emigration into inflamed tissues was almost completely inhibited in $NE^{-/-}$ animals (94% inhibition) whilst

leukocyte adhesion was unaffected **(Figure 3A**). Of note, the percentage of blood circulating neutrophils and key microvascular flow hemodynamic parameters were the same between WT and $NE^{-/-}$ mice (**Supplementary material, Figure S2**). Pre-treatment of WT animals with silvestat also resulted in an inhibition of leukocyte extravasation but not adhesion (**Supplementary material, Figure 3A,B**). Similar results were obtained in a model of mesenteric I/R where $NE^{-/-}$ mice showed no defect in leukocyte adhesion but were profoundly suppressed in terms of leukocyte extravasation into interstitial tissues as compared to WT animals **(Figure 3B, Supplementary material Figure S2, Movie S3)**.

To ascertain if the role of NE is mediating neutrophil breaching of venular walls is driven by a cell-autonomous mechanism involving neutrophil-derived NE (as opposed to tissue-derived NE), we conducted a series of cell transfer experiments in which fluorescently-labeled bone-marrow leukocytes derived from WT and $NE^{-/-}$ mice were injected intravenously into WT or $NE^{-/-}$ recipient animals prior to I/R injury. At the end of the reperfusion period, the transmigration response of donor leukocytes in cremaster muscles was analyzed by confocal microscopy. Donor WT leukocytes showed similar profile of transmigration post I/R injury when injected in WT or $NE^{-/-}$ recipient animals, suggesting that the genetic background of the recipient mouse (i.e. NE deficiency in the vasculature and interstitial tissue) does not account for the defective neutrophil transmigration response noted in $NE^{-/-}$ animals (**Figure 3C**). However, when $NE^{-/-}$ leukocytes were transferred into WT or $NE^{-/-}$ recipient animals, the migration of these donor cells into tissues was significantly suppressed, indicating that the role of NE in the migration of neutrophils through the vessel wall in I/R injury is a cell-autonomous effect.

As breaching the venular wall involves penetrating multiple barriers, including the endothelium and the venular BM [34,35], we next determined the site of arrest of NE-deficient neutrophils within venular walls in whole-mount immunostained tissues using

confocal microscopy. The images showed a significant increase in the number of neutrophils that had breached the endothelium but were retained within the venular wall in $NE^{-/-}$ mice as compared to WT controls post reperfusion period **(Figure 3D,E)**. Similar results were obtained in the model of mesenteric I/R **(Figure 3F).** WT mice pre-treated with the NE inhibitor sivelestat and subjected to cremasteric I/R also showed increased number of neutrophils within the venular wall post breaching of the endothelium, as compared to mice treated with the drug vehicle **(Supplementary material, Figure S3C).**

Collectively these results identify a selective role for neutrophil-derived NE in mediating leukocyte migration through venular walls, a response that appears to occur in a cell-autonomous manner. Furthermore, whilst NE deletion or pharmacological blockade does not impact neutrophil transendothelial migration, NE appears to play an important role in neutrophil breaching of the venular basement membrane post I/R injury.

Neutrophil-derived NE is retained within the venular BM during neutrophil transmigration.

Having found that NE deficiency leads to neutrophil retention at the level of the venular BM in a cell-autonomous manner, we aimed to gain more insight into the mechanism through which this happens. Initially, we determined the localization of NE enzymatic activity and protein expression during the process of neutrophil migration from the vascular lumen into the interstitial space as assessed by immunostaining and analysis of tissues by confocal microscopy. Using a specific NE-fluorescent activatable substrate (NE680FAST) injected i.v., we observed an intense NE activity associated with neutrophils located in the abluminal aspect of the vessel wall (i.e. within the venular BM), and at a lower level in tissue infiltrated leukocytes (**Figure 4A**). Similarly, using a specific antibody

(**Supplementary material, Figure S4**), NE was strongly associated with neutrophils within both the vascular lumen and the venular wall, and, to a lesser extent, in tissue-infiltrated neutrophils **(Figure 3B,C)**. Quantification of neutrophil NE expression at different stages of neutrophil migration through the venular wall demonstrated a significant decrease in the neutrophil-associated NE as the cells moved from the vascular lumen to the interstitial tissue. Specifically, neutrophils within the venular BM and interstitial tissues post I/R injury showed 33.6% and 57.0% reduction in NE expression, as compared to luminal neutrophils, respectively. Interestingly, this response was associated with an increase in NE localization within the BM itself in WT mice subjected to I/R injury but not in $NE^{-/-}$ animals **(Figure 3D)**.

Taken together, these results suggest that during I/R injury, neutrophils release approximately one third of their NE content within the venular BM as they encounter this structure during their emigration into the interstitium.

NE mediates remodeling of the venular BM

We have previously reported on the expression and remodeling of regions within the venular BM that exhibit reduced levels of certain matrix proteins (e.g. collagen IV and laminins) that act as preferred exit portals for transmigrating neutrophils [36,37]. These regions, termed matrix protein low expression regions (LERs), were investigated here in terms of their size by confocal microscopy in cremasteric and mesenteric tissues post I/R injury. Whilst WT mice subjected to I/R showed increased average size of venular BM LERs as compared to sham-treated mice, no such increase was noted in $NE^{-/-}$ animals (**Figure 5A–D**). Pharmacological blockade of NE also suppressed the increase in size of LERs in the cremaster muscle I/R injury model (**Supplementary material, Figure S3D**).

Interestingly, immunostaining of WT tissues with antibodies against neutrophils and venular BM (pan-laminin Ab), demonstrated that ~30% and 50% of tissue infiltrated neutrophils were immunoreactive for laminin in the cremaster muscle and mesenteric I/R models, respectively (**Figure 5E,F**), suggesting carriage of laminin fragments by migrating neutrophils.

Taken together these results demonstrate that NE can facilitate remodeling of the venular BM through increasing the size of neutrophil permissive regions. This remodeling likely occurs through disruption of the laminin network of the BM, as mediated via cleavage and carriage of laminin fragments by the emigrating neutrophils.

NE$^{-/-}$ mice exhibit reduced I/R-induced neutrophil activation and vascular leakage, but also show suppressed recruitment of monocytes and pro-healing M2-macrophages in inflamed tissues.

In a final series of experiments we investigated the potential impact of NE deletion on other key cellular features of I/R injury, namely neutrophil activation, vascular leakage and recruitment of monocytes. The activation state of tissue infiltrated neutrophils (both in the interstitium and vasculature, **Figure 6A**) in sham and I/R injured cremaster muscles of WT and NE-deficient mice was quantified through analyzing levels of reactive oxygen species (ROS) by flow cytometry. Whilst neutrophils present in WT cremaster muscles exhibited an enhanced DHE signal (**Figure 6B**) (and higher CD11b expression, MFI = 21732±4389 versus 14276±1335 for I/R versus sham-operated group, respectively) as compared to cells in sham-operated tissues or blood leukocytes, the few neutrophils found in NE$^{-/-}$ tissues (mainly within the vasculature and the venular wall (Figure 3 and Figure 6A) had a reduced DHE signal (**Figure 6A,B**). The suppressed activation state of NE$^{-/-}$ tissue

neutrophils was associated with reduced vascular leakage in the KO mice post I/R injury, as compared to the response noted in WT animals **(Figure 6C)**. Interestingly however, in assessing the impact of NE deficiency on the resolution phase of the I/R injury, whilst both monocyte and M2 macrophage numbers were elevated in WT cremaster muscles at 20 h post-reperfusion (**Figure 6D,E**), these responses were markedly inhibited in $NE^{-/-}$ animals. Of note, local I/R insult had no impact on blood monocyte numbers in either WT on $NE^{-/-}$ animals (**supplementary material, Figure S5**).

Collectively, these results suggest that although blocking NE-dependent neutrophil extravasation may be an effective strategy at reducing the number and activation state of tissue infiltrated neutrophils, such an intervention may also affect the recruitment of tissue healing immune cells such as monocytes and M2 macrophages.

DISCUSSION

The migration of neutrophils from the blood stream into inflamed tissues is a tightly regulated process essential for the rapid development of an effective immune response against injury and invading pathogens. This phenomenon, extensively studied during physiological responses in healthy tissues [34,35,38], is also a key element in the development of many acute and life-threatening inflammatory pathologies [39,40] such as I/R injury [11-13,15]. Several therapeutic strategies have been tested both in pre-clinical and clinical studies of inflammatory conditions to inhibit neutrophil recruitment and/or functions through the use of natural or synthetic (e.g. sivelestat) inhibitors of NE [26,41]. The use of sivelestat in particular confirmed the potential of targeting NE for the treatment of disorders such as acute lung injury [42], complications arising from myocardial surgery [43], organ transplantation [44] and several model of ischemia reperfusion injury [45-47]. However, at present the specific role(s) of NE in I/R injury remains poorly understood. To address this issue, here we have comprehensively studied the role of NE in neutrophil migration in multiple murine models of I/R injury using both genetic deletion and pharmacological inhibition. Our findings provide univocal evidence for a vital and non-redundant role for NE in mediating neutrophil tissue infiltration post I/R and categorically identify breaching and remodeling of the venular BM as a key site of action of NE in this process. However, our results also indicate that suppressing NE can lead to reduced tissue infiltration of wound healing immune cells, highlighting a need for better understanding of the mechanisms of actions of NE inhibitors.

Early studies suggested that NE was a key candidate for the regulation of neutrophil recruitment at sites of I/R injury, though such works failed to fully establish the associated mechanisms [48]. NE can potentially impact the migration of neutrophils through blood vessel walls at multiple levels. For example, NE can cleave cell-adhesion (e.g. ICAM-1) [49] and junctional (e.g. JAM-C) [50] molecules present on the endothelium, pro-inflammatory cell surface receptors (e.g. TLR4, PAR-2) [51,52], and components of the venular BM (e.g. elastin, laminins) [53]. NE can also regulate the bioactivity and/or bioavailability of numerous pro-inflammatory cytokines (TNF) and chemokines (IL-8) [54,55]. Here we studied NE in the context of I/R injury as induced in the myocardium, kidneys, mesentery and cremaster muscles. In all models, a dramatic suppression of tissue-infiltration of neutrophils was noted, with some indications of concomitant inhibition of acute tissue injury. Similar results were obtained using an NE inhibitor, observations that are in agreement with previously published works using different models of I/R injury [45-47] and confirming the efficacy of sivelestat in the treatment of perioperative acute inflammatory responses in the clinic [42,43]. In sharp contrast, the use of NE-deficient mice have led to conflicting and varied results regarding the functions of this protease in neutrophil infiltration, questioning the efficacy and specificity of existing NE inhibitors. Several reports have shown that $NE^{-/-}$ mice can exhibit a normal neutrophil transmigration response in models of bacterial infections [29] or in reductive experimental models of tissue inflammation as induced by bacterial derived products (LPS), cytokines (TNF, IL-1β) [27],[36], or neutrophil-chemoattractants (LTB_4) [56]. Such conflicting results may suggest the existence of compensatory mechanisms in $NE^{-/-}$ mice as mediated via the actions of other serine proteases (e.g. PR3) with similar functions to that noted with NE. In support of such a possibility we have previously shown that a broad-spectrum serine protease inhibitor can suppress IL-1β-induced neutrophil transmigration in both WT and $NE^{-/-}$ mice [56]. Divergent impacts of NE deficiency could also be attributed to differing

mechanisms of action of NE in distinct inflammatory scenarios. For example, the suppression of neutrophil recruitment in NE-deficient mice within a zymozan-induced peritonitis model was aligned with reduced generation of the pro-inflammatory chemokines CXCL1 and CCL3 [27]. Of note, within the cremaster muscle I/R model employed here, whilst significant suppression of neutrophil recruitment was observed in $NE^{-/-}$ animals, this was not mediated through reduced levels of endogenous chemokines (e.g. CXCL1 or CCL2; data not shown). Overall, considering the broad substrate specificity of NE, and the wide range of stimuli that can induce its release and/or cell surface expression on neutrophils, it is not inconceivable that NE shows different functions and efficacy in regulating neutrophil trafficking as governed by the nature and severity of the inflammatory trigger.

To investigate what stage of neutrophil trafficking NE supported post I/R, we analyzed the dynamics of neutrophil responses in I/R injured cremaster muscles and mesenteric tissues of WT and $NE^{-/-}$ mice by intravital microscopy. These studies identified a selective role for NE in mediating neutrophil breaching of venular walls. Interestingly, adoptive transfer of neutrophils deficient in NE into WT mice led to suppression of neutrophil migration, providing direct evidence for the ability of neutrophil-derived NE in supporting neutrophil trafficking in a cell autonomous manner. In addition to proteases, previous studies have shown that neutrophil-derived LTB_4 can act in a feed-forward manner to support a collective directional motility phenomenon within interstitial tissues known as swarming [57]. As well as providing chemotactic cues, cell autonomous pathways can regulate neutrophil polarity and migration, such as that reported for neutrophil-derived ATP and its hydrolyzed form, adenosine [58], and neutrophil-expressed junctional adhesion molecule-A (JAM-A) [59].

Having identified breaching of venular walls as the site of arrest of NE-deficient neutrophils, detailed analysis of I/R injured tissues indicated that $NE^{-/-}$ neutrophils were unable to penetrate the vascular basement membrane. The latter is a critical step in neutrophil breaching of the venular wall and subsequent migration into the interstitial tissue [35]. Disruption of venular basement membrane following neutrophil transmigration was first demonstrated *in vitro* [60], though the associated mechanisms remained elusive for many years. Significant insight to this phase of neutrophil trafficking was provided by our previous works where we identified regions within the venular BM that exhibit lower deposition of certain matrix proteins, such as collagen IV and laminins [36,37]. Functionally, these regions are the preferred sites of neutrophil egress through the venular BM, and are remodeled by transmigrating neutrophils in terms of their size and protein content upon cytokine and chemokine-induced inflammation in a strictly neutrophil-dependent manner [36,37]. These specialized venular wall regions termed matrix protein low expression regions (LERs) are now accepted as a key element of neutrophil trafficking [61-63]. In the current study we noted that NE-mediated neutrophil migration through venular walls involves remodeling of the LERs. These findings are supported by *in vitro* studies showing that NE can cleave extracellular matrix proteins such as laminin [53] and collagen [64]. In mediating breaching of the venular BM, it is plausible to consider that NE achieves this through localized expression on the cell surface of migrating neutrophils. Indeed, NE can be expressed at the cell surface of neutrophils upon stimulation [56] through its binding to negatively-charged glyocoproteins [65] or via its interaction with the leukocyte integrin MAC-1 [50,66]. In the present study, the use of an NE-specific fluorescent activatable substrate indicated the association of NE activity with neutrophils within the abluminal aspect of the vessel wall of cremaster muscles. These findings support the concept that membrane-bound NE is critical in facilitating NE-mediated

functions as it renders the enzyme resistant to endogenous inhibition[67]. Another example of this is the role of NE in supporting the aberrant mode of neutrophil transendothelial migration (TEM), neutrophil reverse TEM, i.e. movement within endothelial cell junctions in an abluminal to luminal direction [68]. This junctional reverse motility response of neutrophils was most pronounced following I/R injury [68] and was mechanistically linked with NE-mediated cleavage of the endothelial cell tight junctional molecule JAM-C via its binding to neutrophil Mac-1 *in vivo* [50]. In the present study, we observed that in addition to be being cell surface expressed, NE was also released within the venular BM during neutrophil extravasation. Interestingly, the remodeling of LERs in the cremaster muscle and mesenteric I/R injury models was associated with the presence of a subpopulation of tissue-infiltrated neutrophils that were immunostained for laminin. Collectively these results suggest that neutrophils can remodel the venular BM LERs through localized cell surface expression of NE and/or localized release of NE within the venular BM. The former could lead to neutrophils carrying fragments of venular BM laminin, possibly via their cell surface expression of laminin-binding receptor α6β1 integrin, as we have previously described [69,70].

Having found that functional blockade of NE retains neutrophils within venular walls in I/R-stimulated tissues, and considering the relevance of these findings to future therapeutic use of NE blockers, we sought to investigate if such a vascular retention phenomena could have detrimental vascular/tissue effects. In addressing this notion, the activation state of tissue infiltrated neutrophils and vascular permeability in WT and $NE^{-/-}$ mice was quantified. These studies showed reduced neutrophil activation, as measured through ROS generation, and vascular leakage in $NE^{-/-}$ mice, suggesting that retention of potentially activated neutrophils within the venular wall does not impede vascular barrier integrity. However, in assessing the resolution phase of I/R injury, we noted that NE-genetic deficiency was associated with reduced recruitment of monocytes and M2

macrophages. These findings are in line with the notion that neutrophil diapedesis can mediate monocyte migration [71,72] and can promote macrophage polarization towards a pro-healing phenotype [73].

Collectively, our findings demonstrate a selective and non-redundant role for NE in I/R-induced neutrophil migration through venular walls as mediated via the remodeling of the venular BM. However, whilst the results suggest that NE inhibitors maybe useful strategies in suppressing acute neutrophil-mediated tissue damage post I/R, the findings also raise caution for the use of such drugs as blockade of neutrophil migration may compromise the tissue repair process via inhibiting recruitment of pro-healing immune cells.

ACKNOWLEDGMENTS

The authors would like to thank Professor S Shapiro for providing the NE-deficient mice, Dr Nancy Hogg for providing the anti-mouse MRP-14 mAb and Dr Matthew Golding for his helpful assessment with the manuscript.

FUNDING

This work was supported by grants from the British Heart Foundation: PG/03/123/16102 (SN and M-B V), FS/11/19/28761 (WA) and FS/05/078/19406 (LG and PM), the Wellcome Trust: 098291/Z/12/Z and 101604/Z/13/Z (SN), and Arthritis Research UK: 19913 (M-B V).

Author contributions statement

M-B V designed and performed most experiments, analyzed data, and contributed to the writing of the manuscript; GL designed and performed the myocardial I/R experiments and mesenteric I/R IVM; AW designed and performed the cremaster muscle I/R IVM; LL assisted with image acquisition and analysis of myocardial I/R experiment; NP, RDP and SC designed and performed the mesenteric I/R experiments and data analysis; SN provided overall project supervision, contributed to the design of experiments and the writing of the manuscript.

REFERENCES

1. Chen F, Date H. Update on ischemia-reperfusion injury in lung transplantation. *Curr Opin Organ Transplant* 2015; **20**: 515-520.
2. Ferrari R, Balla C, Malagu M*, et al.* Reperfusion Damage- A Story of Success, Failure, and Hope. *Circ J* 2017; **81**: 131-141.
3. Mizuma A, Yenari MA. Anti-Inflammatory Targets for the Treatment of Reperfusion Injury in Stroke. *Front Neurol* 2017; **8**: 467.
4. Salvadori M, Rosso G, Bertoni E. Update on ischemia-reperfusion injury in kidney transplantation: Pathogenesis and treatment. *World J Transplant* 2015; **5**: 52-67.
5. Granger DN, Kvietys PR. Reperfusion therapy-What's with the obstructed, leaky and broken capillaries? *Pathophysiology* 2017; **24**: 213-228.
6. Eltzschig HK, Eckle T. Ischemia and reperfusion--from mechanism to translation. *Nat Med* 2011; **17**: 1391-1401.
7. Petrovic-Djergovic D, Goonewardena SN, Pinsky DJ. Inflammatory Disequilibrium in Stroke. *Circ Res* 2016; **119**: 142-158.
8. Tecchio C, Cassatella MA. Neutrophil-derived chemokines on the road to immunity. *Semin Immunol* 2016; **28**: 119-128.
9. Tecchio C, Micheletti A, Cassatella MA. Neutrophil-derived cytokines: facts beyond expression. *Front Immunol* 2014; **5**: 508.
10. Winterbourn CC, Kettle AJ, Hampton MB. Reactive Oxygen Species and Neutrophil Function. *Annu Rev Biochem* 2016; **85**: 765-792.
11. Albadawi H, Oklu R, Raacke Malley RE*, et al.* Effect of DNase I treatment and neutrophil depletion on acute limb ischemia-reperfusion injury in mice. *J Vasc Surg* 2016; **64**: 484-493.
12. Garcia-Prieto J, Villena-Gutierrez R, Gomez M*, et al.* Neutrophil stunning by metoprolol reduces infarct size. *Nat Commun* 2017; **8**: 14780.

13. Klausner JM, Paterson IS, Goldman G*, et al.* Postischemic renal injury is mediated by neutrophils and leukotrienes. *Am J Physiol* 1989; **256**: F794-802.
14. Sawa Y, Matsuda H. Myocardial protection with leukocyte depletion in cardiac surgery. *Semin Thorac Cardiovasc Surg* 2001; **13**: 73-81.
15. Wang K, Wen S, Jiao J*, et al.* IL-21 promotes myocardial ischaemia/reperfusion injury through the modulation of neutrophil infiltration. *Br J Pharmacol* 2017.
16. Rabb H, Mendiola CC, Dietz J*, et al.* Role of CD11a and CD11b in ischemic acute renal failure in rats. *Am J Physiol* 1994; **267**: F1052-1058.
17. Kelly KJ, Williams WW, Jr., Colvin RB*, et al.* Intercellular adhesion molecule-1-deficient mice are protected against ischemic renal injury. *J Clin Invest* 1996; **97**: 1056-1063.
18. Hager M, Cowland JB, Borregaard N. Neutrophil granules in health and disease. *J Intern Med* 2010; **268**: 25-34.
19. Faurschou M, Borregaard N. Neutrophil granules and secretory vesicles in inflammation. *Microbes Infect* 2003; **5**: 1317-1327.
20. Lee WL, Downey GP. Leukocyte elastase: physiological functions and role in acute lung injury. *Am J Respir Crit Care Med* 2001; **164**: 896-904.
21. Pham CT. Neutrophil serine proteases: specific regulators of inflammation. *Nat Rev Immunol* 2006; **6**: 541-550.
22. Papayannopoulos V, Metzler KD, Hakkim A*, et al.* Neutrophil elastase and myeloperoxidase regulate the formation of neutrophil extracellular traps. *J Cell Biol* 2010; **191**: 677-691.
23. Vila N, Elena M, Deulofeu R*, et al.* Polymorphonuclear leukocyte elastase in patients with stroke. *Acta Neurol Scand* 1999; **100**: 391-394.

24. Shapiro SD, Ingenito EP. The pathogenesis of chronic obstructive pulmonary disease: advances in the past 100 years. *Am J Respir Cell Mol Biol* 2005; **32**: 367-372.

25. Smith FB, Fowkes FG, Rumley A*, et al.* Tissue plasminogen activator and leucocyte elastase as predictors of cardiovascular events in subjects with angina pectoris: Edinburgh Artery Study. *Eur Heart J* 2000; **21**: 1607-1613.

26. Henriksen PA. The potential of neutrophil elastase inhibitors as anti-inflammatory therapies. *Curr Opin Hematol* 2014; **21**: 23-28.

27. Young RE, Thompson RD, Larbi KY*, et al.* Neutrophil elastase (NE)-deficient mice demonstrate a nonredundant role for NE in neutrophil migration, generation of proinflammatory mediators, and phagocytosis in response to zymosan particles in vivo. *J Immunol* 2004; **172**: 4493-4502.

28. Belaaouaj A, McCarthy R, Baumann M*, et al.* Mice lacking neutrophil elastase reveal impaired host defense against gram negative bacterial sepsis. *Nat Med* 1998; **4**: 615-618.

29. Hirche TO, Atkinson JJ, Bahr S*, et al.* Deficiency in neutrophil elastase does not impair neutrophil recruitment to inflamed sites. *Am J Respir Cell Mol Biol* 2004; **30**: 576-584.

30. Kawabata K, Suzuki M, Sugitani M*, et al.* ONO-5046, a novel inhibitor of human neutrophil elastase. *Biochem Biophys Res Commun* 1991; **177**: 814-820.

31. Miles AA, Miles EM. Vascular reactions to histamine, histamine-liberator and leukotaxine in the skin of guinea-pigs. *J Physiol* 1952; **118**: 228-257.

32. Thompson RD, Noble KE, Larbi KY*, et al.* Platelet-endothelial cell adhesion molecule-1 (PECAM-1)-deficient mice demonstrate a transient and cytokine-specific role for PECAM-1 in leukocyte migration through the perivascular basement membrane. *Blood* 2001; **97**: 1854-1860.

33. Woodfin A, Reichel CA, Khandoga A*, et al.* JAM-A mediates neutrophil transmigration in a stimulus-specific manner in vivo: evidence for sequential roles for JAM-A and PECAM-1 in neutrophil transmigration. *Blood* 2007; **110**: 1848-1856.

34. Nourshargh S, Hordijk PL, Sixt M. Breaching multiple barriers: leukocyte motility through venular walls and the interstitium. *Nat Rev Mol Cell Biol* 2010; **11**: 366-378.

35. Voisin MB, Nourshargh S. Neutrophil transmigration: emergence of an adhesive cascade within venular walls. *J Innate Immun* 2013; **5**: 336-347.

36. Wang S, Voisin MB, Larbi KY*, et al.* Venular basement membranes contain specific matrix protein low expression regions that act as exit points for emigrating neutrophils. *J Exp Med* 2006; **203**: 1519-1532.

37. Voisin MB, Probstl D, Nourshargh S. Venular basement membranes ubiquitously express matrix protein low-expression regions: characterization in multiple tissues and remodeling during inflammation. *Am J Pathol* 2010; **176**: 482-495.

38. Nourshargh S, Alon R. Leukocyte migration into inflamed tissues. *Immunity* 2014; **41**: 694-707.

39. van der Linden M, Meyaard L. Fine-tuning neutrophil activation: Strategies and consequences. *Immunol Lett* 2016; **178**: 3-9.

40. Kolaczkowska E, Kubes P. Neutrophil recruitment and function in health and inflammation. *Nat Rev Immunol* 2013; **13**: 159-175.

41. Williams SE, Brown TI, Roghanian A*, et al.* SLPI and elafin: one glove, many fingers. *Clin Sci (Lond)* 2006; **110**: 21-35.

42. Nomura N, Asano M, Saito T*, et al.* Sivelestat attenuates lung injury in surgery for congenital heart disease with pulmonary hypertension. *Ann Thorac Surg* 2013; **96**: 2184-2191.

43. Inoue N, Oka N, Kitamura T*, et al.* Neutrophil elastase inhibitor sivelestat attenuates perioperative inflammatory response in pediatric heart surgery with cardiopulmonary bypass. *Int Heart J* 2013; **54**: 149-153.

44. Harada M, Oto T, Otani S*, et al.* A neutrophil elastase inhibitor improves lung function during ex vivo lung perfusion. *Gen Thorac Cardiovasc Surg* 2015; **63**: 645-651.

45. Uchida Y, Freitas MC, Zhao D*, et al.* The protective function of neutrophil elastase inhibitor in liver ischemia/reperfusion injury. *Transplantation* 2010; **89**: 1050-1056.

46. Fujimura N, Obara H, Suda K*, et al.* Neutrophil elastase inhibitor improves survival rate after ischemia reperfusion injury caused by supravisceral aortic clamping in rats. *J Surg Res* 2013; **180**: e31-36.

47. Sakai S, Tajima H, Miyashita T*, et al.* Sivelestat sodium hydrate inhibits neutrophil migration to the vessel wall and suppresses hepatic ischemia-reperfusion injury. *Dig Dis Sci* 2014; **59**: 787-794.

48. Zimmerman BJ, Granger DN. Reperfusion-induced leukocyte infiltration: role of elastase. *Am J Physiol* 1990; **259**: H390-394.

49. Champagne B, Tremblay P, Cantin A*, et al.* Proteolytic cleavage of ICAM-1 by human neutrophil elastase. *J Immunol* 1998; **161**: 6398-6405.

50. Colom B, Bodkin JV, Beyrau M*, et al.* Leukotriene B4-Neutrophil Elastase Axis Drives Neutrophil Reverse Transendothelial Cell Migration In Vivo. *Immunity* 2015; **42**: 1075-1086.

51. Devaney JM, Greene CM, Taggart CC*, et al.* Neutrophil elastase up-regulates interleukin-8 via toll-like receptor 4. *FEBS Lett* 2003; **544**: 129-132.

52. Muley MM, Reid AR, Botz B*, et al.* Neutrophil elastase induces inflammation and pain in mouse knee joints via activation of proteinase-activated receptor-2. *Br J Pharmacol* 2016; **173**: 766-777.

53. Mydel P, Shipley JM, Adair-Kirk TL*, et al.* Neutrophil elastase cleaves laminin-332 (laminin-5) generating peptides that are chemotactic for neutrophils. *J Biol Chem* 2008; **283**: 9513-9522.

54. Walsh DE, Greene CM, Carroll TP*, et al.* Interleukin-8 up-regulation by neutrophil elastase is mediated by MyD88/IRAK/TRAF-6 in human bronchial epithelium. *J Biol Chem* 2001; **276**: 35494-35499.

55. Benabid R, Wartelle J, Malleret L*, et al.* Neutrophil elastase modulates cytokine expression: contribution to host defense against Pseudomonas aeruginosa-induced pneumonia. *J Biol Chem* 2012; **287**: 34883-34894.

56. Young RE, Voisin MB, Wang S*, et al.* Role of neutrophil elastase in LTB4-induced neutrophil transmigration in vivo assessed with a specific inhibitor and neutrophil elastase deficient mice. *Br J Pharmacol* 2007; **151**: 628-637.

57. Lammermann T, Afonso PV, Angermann BR*, et al.* Neutrophil swarms require LTB4 and integrins at sites of cell death in vivo. *Nature* 2013; **498**: 371-375.

58. Chen Y, Corriden R, Inoue Y*, et al.* ATP release guides neutrophil chemotaxis via P2Y2 and A3 receptors. *Science* 2006; **314**: 1792-1795.

59. Cera MR, Fabbri M, Molendini C*, et al.* JAM-A promotes neutrophil chemotaxis by controlling integrin internalization and recycling. *J Cell Sci* 2009; **122**: 268-277.

60. Huber AR, Weiss SJ. Disruption of the subendothelial basement membrane during neutrophil diapedesis in an in vitro construct of a blood vessel wall. *J Clin Invest* 1989; **83**: 1122-1136.

61. Poduval P, Sillat T, Virtanen I*, et al.* Abnormal basement membrane type IV collagen alpha-chain composition in labial salivary glands in Sjogren's syndrome. *Arthritis Rheum* 2009; **60**: 938-945.

62. Reichel CA, Rehberg M, Bihari P*, et al.* Gelatinases mediate neutrophil recruitment in vivo: evidence for stimulus specificity and a critical role in collagen IV remodeling. *J Leukoc Biol* 2008; **83**: 864-874.

63. Reichel CA, Rehberg M, Lerchenberger M*, et al.* Ccl2 and Ccl3 mediate neutrophil recruitment via induction of protein synthesis and generation of lipid mediators. *Arterioscler Thromb Vasc Biol* 2009; **29**: 1787-1793.

64. Weathington NM, van Houwelingen AH, Noerager BD*, et al.* A novel peptide CXCR ligand derived from extracellular matrix degradation during airway inflammation. *Nat Med* 2006; **12**: 317-323.

65. Campbell EJ, Owen CA. The sulfate groups of chondroitin sulfate- and heparan sulfate-containing proteoglycans in neutrophil plasma membranes are novel binding sites for human leukocyte elastase and cathepsin G. *J Biol Chem* 2007; **282**: 14645-14654.

66. Cai TQ, Wright SD. Human leukocyte elastase is an endogenous ligand for the integrin CR3 (CD11b/CD18, Mac-1, alpha M beta 2) and modulates polymorphonuclear leukocyte adhesion. *J Exp Med* 1996; **184**: 1213-1223.

67. Owen CA, Campbell MA, Sannes PL*, et al.* Cell surface-bound elastase and cathepsin G on human neutrophils: a novel, non-oxidative mechanism by which neutrophils focus and preserve catalytic activity of serine proteinases. *J Cell Biol* 1995; **131**: 775-789.

68. Woodfin A, Voisin MB, Beyrau M*, et al.* The junctional adhesion molecule JAM-C regulates polarized transendothelial migration of neutrophils in vivo. *Nat Immunol* 2011; **12**: 761-769.

69. Dangerfield JP, Wang S, Nourshargh S. Blockade of alpha6 integrin inhibits IL-1beta- but not TNF-alpha-induced neutrophil transmigration in vivo. *J Leukoc Biol* 2005; **77**: 159-165.

70. Wang S, Dangerfield JP, Young RE*, et al.* PECAM-1, alpha6 integrins and neutrophil elastase cooperate in mediating neutrophil transmigration. *J Cell Sci* 2005; **118**: 2067-2076.

71. Soehnlein O, Zernecke A, Eriksson EE*, et al.* Neutrophil secretion products pave the way for inflammatory monocytes. *Blood* 2008; **112**: 1461-1471.

72. Wantha S, Alard JE, Megens RT*, et al.* Neutrophil-derived cathelicidin promotes adhesion of classical monocytes. *Circ Res* 2013; **112**: 792-801.

73. Horckmans M, Ring L, Duchene J*, et al.* Neutrophils orchestrate post-myocardial infarction healing by polarizing macrophages towards a reparative phenotype. *Eur Heart J* 2017; **38**: 187-197.

74. Hobbs JA, May R, Tanousis K, et al.* Myeloid cell function in MRP-14 (S100A9) null mice. *Mol Cell Biol* 2003; **23**: 2564-2576.

75. Brines M, Patel NS, Villa P, et al.* Nonerythropoietic, tissue-protective peptides derived from the tertiary structure of erythropoietin. *Proc Natl Acad Sci U S A* 2008; **105**: 10925-10930.

*76. Patel NS, Cuzzocrea S, Chatterjee PK, et al. Reduction of renal ischemia-reperfusion injury in 5-lipoxygenase knockout mice and by the 5-lipoxygenase inhibitor zileuton. Mol Pharmacol 2004; 66: 220-227.

*77. Voisin MB, Woodfin A, Nourshargh S. Monocytes and neutrophils exhibit both distinct and common mechanisms in penetrating the vascular basement membrane in vivo. *Arterioscler Thromb Vasc Biol* 2009; **29**: 1193-1199.

* Cited only in supplementary material.

FIGURE LEGENDS

Figure 1. Neutrophil recruitment into the area at risk of neutrophil elastase deficient mice is impaired following myocardial infarction and reperfusion injury.

(**A)** Reconstructed tiling images of myocardial cryosections acquired by confocal microscopy from wildtype (WT) animals and neutrophil elastase deficient mice ($NE^{-/-}$) and subjected to 25 min of myocardial infarction followed by 2 h of reperfusion (I/R). Tissue sections from sham-operated WT (left panels), I/R-subjected WT (middle panels) and I/R-subjected $NE^{-/-}$ (right panels) animals were immunostained for collagen type IV (red). The yellow box exemplify the ischemic and reperfused region of the left ventricle (area at risk). (**B**) Quantification of the Collagen type IV mean intensity in area at risk (yellow box from (**A**)). (**C**) Confocal images of the area at risk (delimited by the dotted line) from a WT animal subjected to myocardial I/R and immunostained for collagen type IV (red), PECAM-1 (blue) and MRP-14 (green) to visualize the extracellular cellular matrix, blood vasculature and neutrophils, respectively. The image shows neutrophils infiltrating the region at risk only. (**D**) Magnified regions of the region of left ventricle subjected or not to I/R from WT (top panels) and $NE^{-/-}$ (bottom panels) animals. Cryosections were immunostained for collagen type IV (red), PECAM-1 (blue) and MRP-14 (green) to visualize the extracellular cellular matrix, blood vasculature and neutrophils, respectively. Left panels show the three channels together whilst the right panels show the neutrophil channel only. The images exemplify the absence of neutrophil infiltration in the region at risk of the myocardium from $NE^{-/-}$ mice subjected to I/R as compared to WT littermates. The top right panels (WT I/R) are magnified images of the same sample region as shown in (**D**). (**E**) Quantification of the number of neutrophils present in the area at risk. Data represent mean ± SEM from 3 or 4 mice per group. **P<0.01 and *** P<0.001 for

comparison between I/R versus sham-operated animals; and # P<0.05, ### P<0.001 for comparison between WT and $NE^{-/-}$ mice as indicated by lines. Scale bars = 100 µm.

Figure 2. Neutrophil elastase deficient mice are protected from renal ischemia and reperfusion injury.

(**A**) Histopathology of kidney sections from sham-operated WT or WT and $NE^{-/-}$ mouse subjected to renal ischemia/reperfusion and stained with hematoxylin and eosin. The bottom pictures are magnified regions (yellow box) demonstrating the modification of the architectural structure of tubules and glomeruli upon I/R injury in WT but not $NE^{-/-}$ animals. (**B**) Histological score analysis of kidney sections. (**C**) Quantification of the number of PMN infiltrating the kidney. Data represent mean ± SEM from at least 4 animals per group. *** P<0.001 for comparison between I/R versus sham-operated animals; and ### P<0.001 for comparison between WT and $NE^{-/-}$ mice as indicated by lines. Scale bar = 100 µm.

Figure 3. Effect of neutrophil elastase deficiency on leukocyte transmigration responses in post-capillary venules *in vivo* following ischemia/reperfusion injury.

Leukocyte's firm adhesion and transmigration in post-capillary venules of mouse cremaster muscles or mesentery in response to I/R were investigated using intravital microscopy. (**A**) The mouse cremaster muscle from WT and $NE^{-/-}$ animals was surgically exteriorized, superfused with Tyrode's solution and basal leukocyte responses were quantified for 20 min prior to the induction of ischemia using a clamp as detailed in Materials and methods. Thirty minutes later, the clamp on the exteriorized cremaster muscle was removed to induce the reperfusion of the vessels. Leukocyte adhesion (left panel) and extravasation (right panel) responses were quantified at regular intervals for

120 min post reperfusion. For each genotype, a sham-operated group was also analyzed (exteriorized cremaster tissues without the clamp). (**B**) WT and $NE^{-/-}$ mice were subjected to occlusion of the superior mesenteric artery for 35 min, followed by 90 min reperfusion. For each genotype, a sham-treatment group was also analyzed, where laparotomy was conducted without the occlusion of the mesenteric arteries. Both leukocyte adhesion (left panel) and transmigration (right panel) responses were quantified in post-capillary venules at 90 min post-reperfusion. (**C**) Bone marrow neutrophils were isolated from WT or $NE^{-/-}$ mice, fluorescently labeled and injected intravenously into WT or NE−/− recipient mice prior to the induction of ischemia and reperfusion of the cremaster muscle as detailed in Materials and methods. At the end of the experiment, tissues where harvested, fixed and immunostained for neutrophils (MRP-14), Data show the quantification of fluorescent donor neutrophils present in the tissue and normalized to the number of blood circulating donor cells. (**D**) The images are representative confocal pictures of post-capillary venules of the cremaster muscles of WT (left panel) and $NE^{-/-}$ (right panel) mice subjected to 30 min of ischemia followed by 120 min of reperfusion of the cremaster muscles. The images show that whilst in WT neutrophils access the interstitial tissue, $NE^{-/-}$ cells are trapped within the venular basement membrane (arrows). (**E**) Quantification of the number of neutrophils present within the venular basement membrane 2 h post-reperfusion of the cremaster muscles. (**F**) Quantification of the number of neutrophils present within the venular basement membrane following 1.5 h post-reperfusion of the mesentery. Figures are representative of 4–7 animals per group. Mean ± SEM. * $P<0.05$, ** $P<0.01$, *** $P<0.001$ for comparison between I/R versus sham-operated animals (or between WT and $NE^{-/-}$ donor cells for the adoptive transfer experiment); and # $P<0.05$, ## $P<0.01$, ### $P<0.001$ for comparison between WT and $NE^{-/-}$ mice as indicated by lines. Bars = 20μm.

Figure 4. NE is mobilized during the migration of neutrophils through the venular basement membrane.

The cremaster muscles and mesentery of WT and $NE^{-/-}$ mice were subjected to temporary ischemia followed by reperfusion. At the end of the reperfusion period, tissues were collected, fixed and immunostained prior to visualization of the samples using confocal microscopy. (**A**) Representative image of a post-capillary venule (CD31, red) of WT and $NE^{-/-}$ animals subjected to I/R injury and demonstrating the association of the enzymatic activity of NE using the NE680FAST fluorescent substrate (blue) with neutrophils (green) present in the abluminal aspect (i.e. BM) of the vessel wall (plain arrows), and at a lesser extent, interstitial neutrophils (dotted arrows). (**B**) Representative confocal image of a post-capillary venule (2 µm longitudinal cross-section from the middle of the vessel, green) from a WT mouse subjected to I/R showing NE expression (red) in the cytoplasmic compartments (blue) of neutrophils. The bottom panels are enlargements of the yellow boxed region showing neutrophils at different stages of their migration route: i.e. luminal (*i*), within the vascular basement membrane (*ii*) or within the interstitial tissue (*iii*). A 5% opacity filter on the MRP14 channel was applied to highlight NE expression in neutrophils on the right panel. (**C**) Quantification of the mean fluorescence intensity of NE expression in neutrophils at the three stages of their migration (as expressed as percentage change over the intensity of NE from luminal neutrophils). (**D**) Quantification of the fluorescence intensity of NE expression within the venular basement membrane form WT and $NE^{-/-}$ animals at 1 h post-reperfusion. Figures are representative of 4–7 animals per group. Mean ± SEM. * $P<0.05$, ** $P<0.01$, *** $P<0.001$, for comparison of the NE intensity (MFI) between BM/interstitial neutrophils versus luminal cells (**C**), or between I/R versus sham-operated animals (**D**); and # $P<0.05$, ## $P<0.01$ for comparison between WT and $NE^{-/-}$ mice as indicated by the line. Bars = 10µm.

Figure 5. Venular basement membrane is remodeled during ischemia/reperfusion injury and transmigrated neutrophils are positive for laminin.

WT and $NE^{-/-}$ mice were subjected to ischemia / reperfusion of their cremaster muscles or mesentery as described in the Material and methods. At the end of the reperfusion period, tissues were collected, fixed and whole-mount immunostained for neutrophils (MRP14) and basement membrane (Laminin-α5 or pan-laminin) prior to visualization of the samples by confocal microscopy. (**A**) Representative images showing the presence of low expression regions (LERs; circles) within the BM (Laminin- α5) of post-capillary venules of mouse cremaster muscles. (**B**) Quantification of the size of the LER within the BM (Laminin- α5) of the cremaster postcapillary venules. (**C**) Representative images showing the presence and remodeling of LERs (circles) within the BM (Laminin- α5) of post-capillary venules of mouse mesentery. (**D**) Quantification of the size of the LER within the BM (Laminin- α5) of the mesenteric postcapillary venules. (**E**) Representative confocal image of a postcapillary venule (from a WT mouse subjected to I/R) showing the presence of laminin positive neutrophils within the interstitial tissue (arrows). The bottom picture shows the staining of Laminin only. (**F**) Quantification of the number on neutrophils present within the venular basement membrane 1.5 h post reperfusion of the mesentery. Figures are representative of 4–7 animals per group. Mean ± SEM. * $P<0.05$**,** ** $P<0.01$, *** $P<0.001$, for comparison between sham and I/R groups; and # $P<0.05$, ### $P<0.001$ for comparison between WT and $NE^{-/-}$ mice as indicated by the line. Bars = 10 µm.

Figure 6. NE-genetic deficiency inhibits neutrophil activation and monocyte/macrophage recruitment.

The cremaster muscles of WT and $NE^{-/-}$ mice were subjected to temporary ischemia followed by reperfusion; and leukocyte phenotype and vascular leakage were quantified by flow cytometry and Evan's blue assay, respectively. (**A**) Quantification of the total number of neutrophils in the cremaster muscles (i.e. interstitial and vascular neutrophils included). (**B**) Quantification of ROS generation by isolated neutrophils from blood or cremaster muscles as measured by DHE mean fluorescence intensity (MFI). (**C**) Quantification of the vascular leakage into the tissue post-reperfusion (4 h). (**D**) Quantification of total number of monocytes in the cremaster muscles at 20 h post reperfusion. (**E**) Quantification of the total number of M2 (CD206+) macrophages in the cremaster muscles at 20 h post reperfusion. Data represent mean ± SEM from 4–6 mice per group (from 3 independent experiments). * $P<0.05$, ** $P<0.01$, for comparison between sham and I/R groups; and # $P<0.05$, ## $P<0.01$ for comparison between WT and $NE^{-/-}$ mice as indicated by the line.

SUPPLEMENTARY MATERIAL ONLINE

Supplementary materials and methods **YES, all within the same combined file with Suppl Figures**

Supplementary figure and movie legends **YES, all within the same combined file with Suppl Figures**

Figure S1. Assessment of renal dysfunction following kidney ischemia***/***reperfusion injury (I/R injury)

Figure S2. Assessment of blood neutrophils, vessel diameter and hemodynamics of postcapillary venules in WT and $NE^{-/-}$ animals

Figure S3. Pharmacological inhibition of neutrophil elastase blocks the migration of neutrophils at the level of the basement membrane post I/R injury

Figure S4. Specificity of a new rabbit anti-mouse NE antibody

Figure S5. Assessment of blood monocytes of WT and $NE^{-/-}$ animals following I/R injury

Movie S1. Bright-field intravital microscopy of the $NE^{-/-}$ cremaster muscle subjected to ischemia***/***reperfusion injury

Movie S2. Bright-field intravital microscopy of the $NE^{-/-}$ cremaster muscle subjected to ischemia***/***reperfusion injury

Movie S3. Bright-field intravital microscopy of the mesenteric tissue subjected to ischemia***/***reperfusion injury

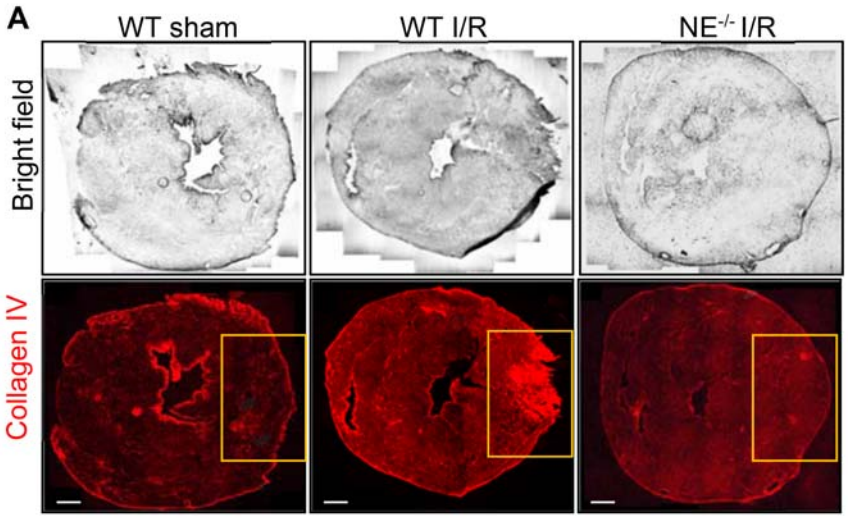
A
WT sham
WT I/R
NE-/- I/R
Bright field
Collagen IV

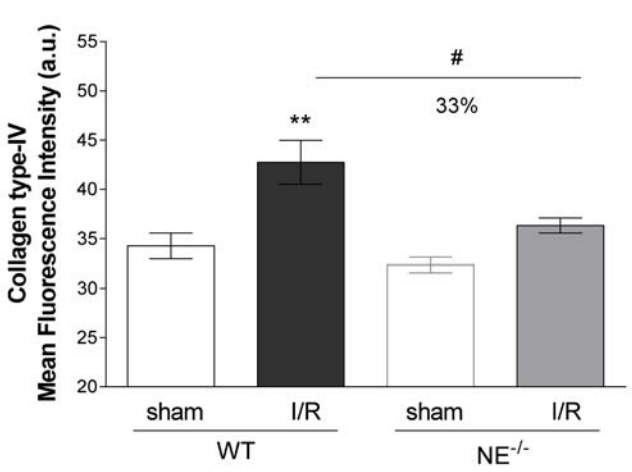
B
Collagen type-IV
Mean Fluorescence Intensity (a.u.)
55
50
45
40
35
30
25
20
#
33%
**
sham
I/R
sham
I/R
WT
NE-/-

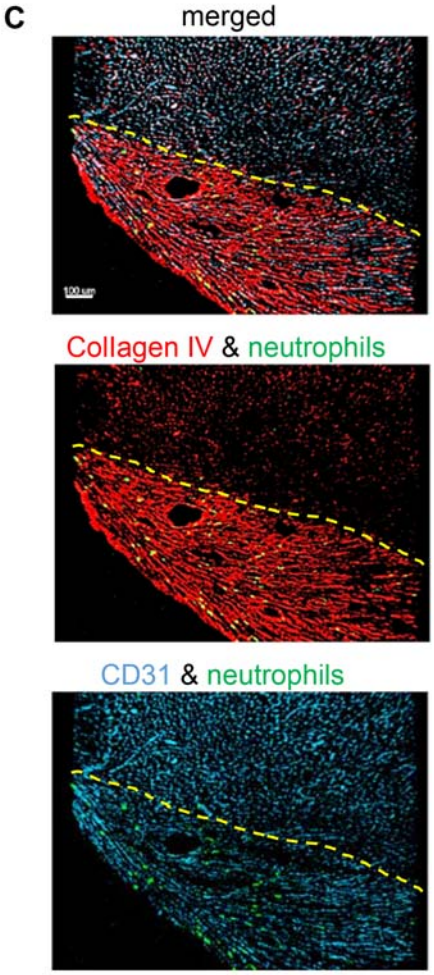
C
merged
100 um
Collagen IV & neutrophils
CD31 & neutrophils

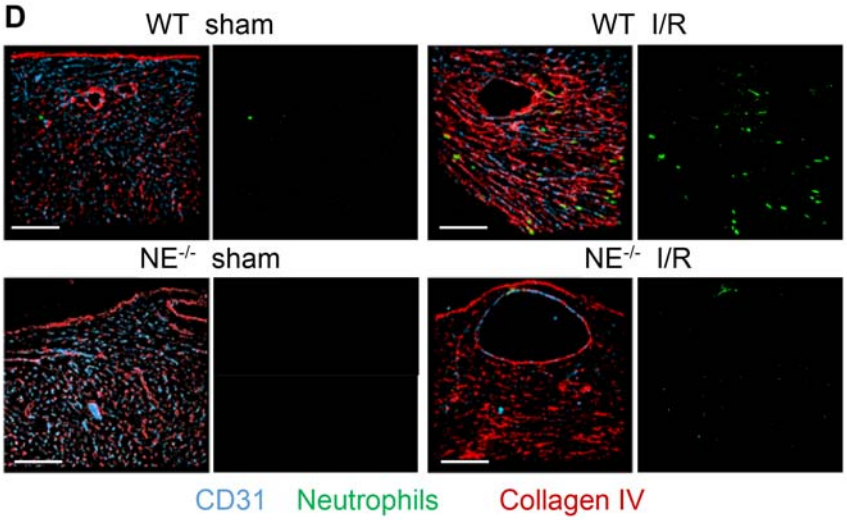
D
WT sham
WT I/R
NE-/- sham
NE-/- I/R
CD31
Neutrophils
Collagen IV

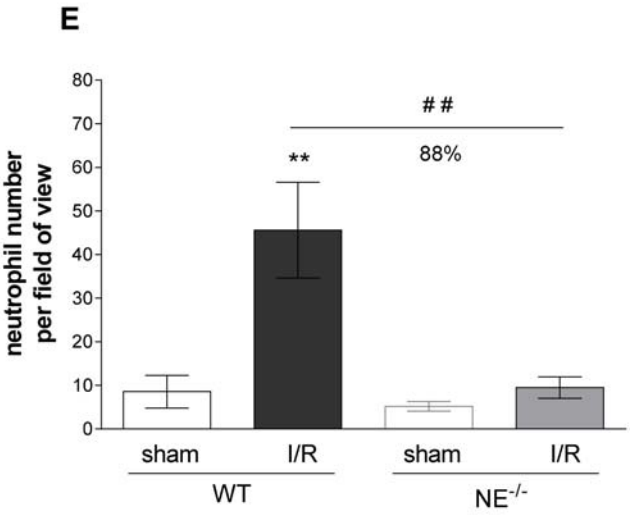
E
neutrophil number
per field of view
80
70
60
50
40
30
20
10
0
# #
88%
**
sham
I/R
sham
I/R
WT
NE-/-

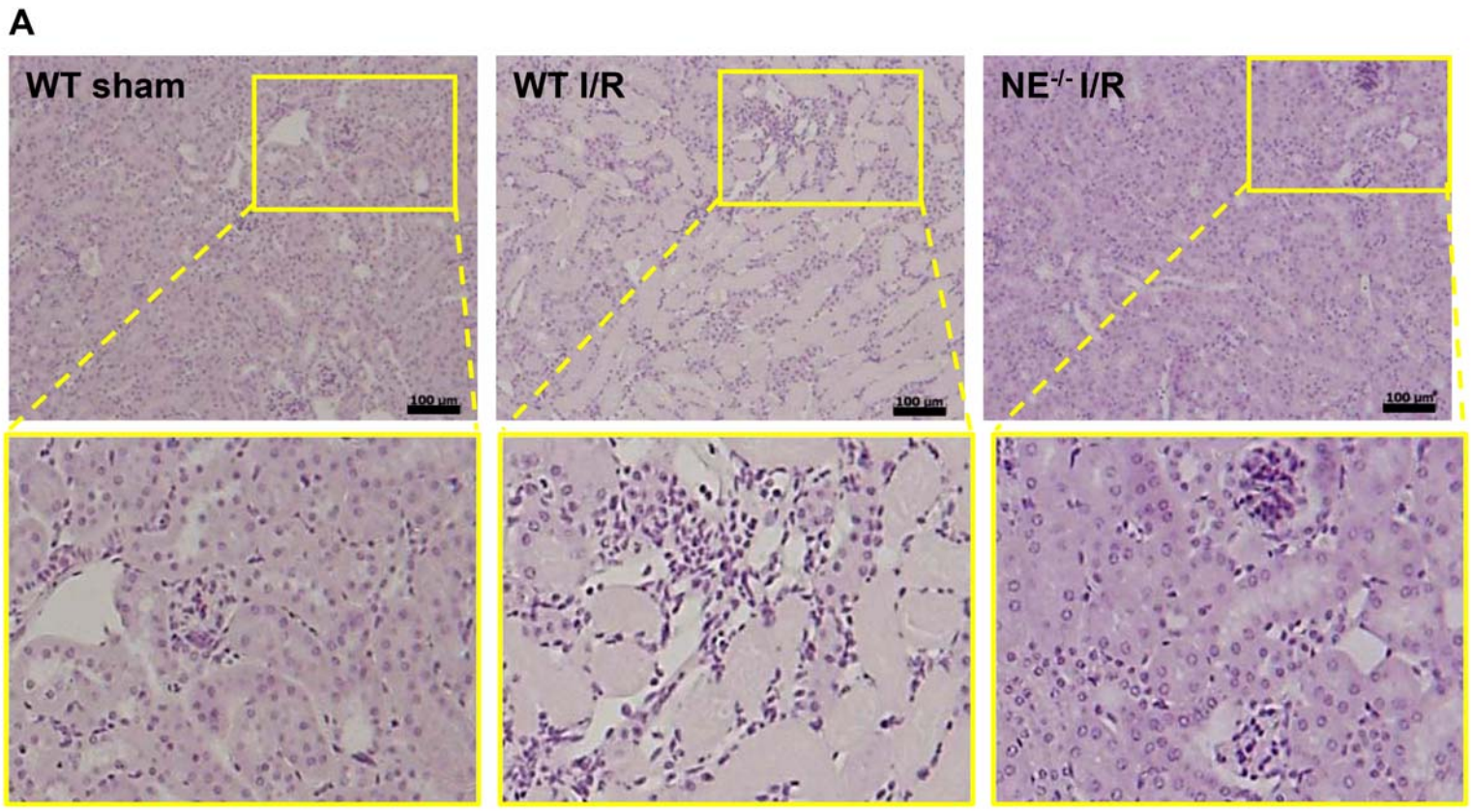
A
WT sham
WT I/R
NE-/- I/R
100 µm
100 µm
100 µm

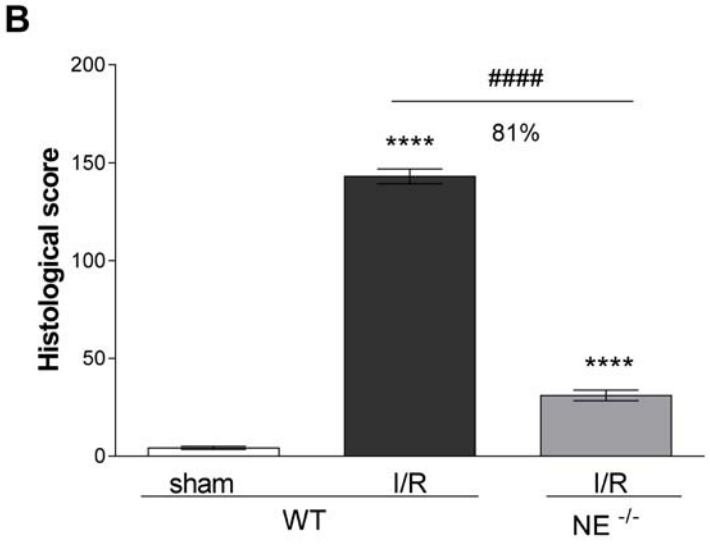
B
Histological score
200
150
100
50
0
####
81%
****
****
sham
I/R
I/R
WT
NE -/-

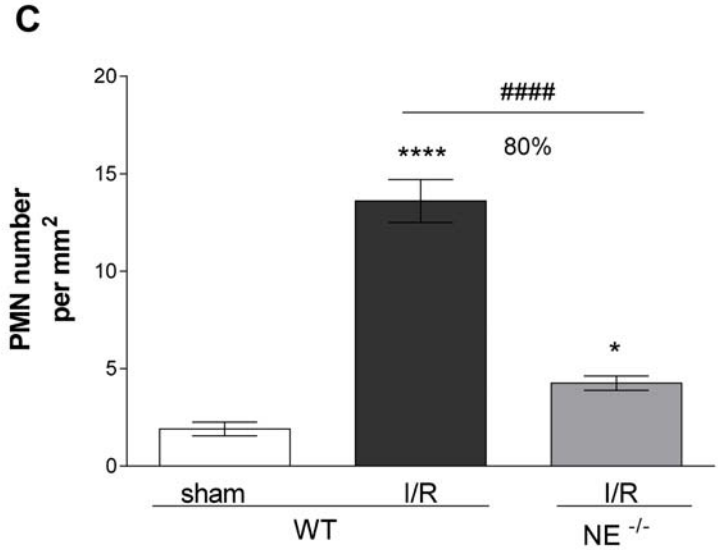
C
PMN number per mm2
20
15
10
5
0
####
80%
****
*
sham
I/R
I/R
WT
NE -/-

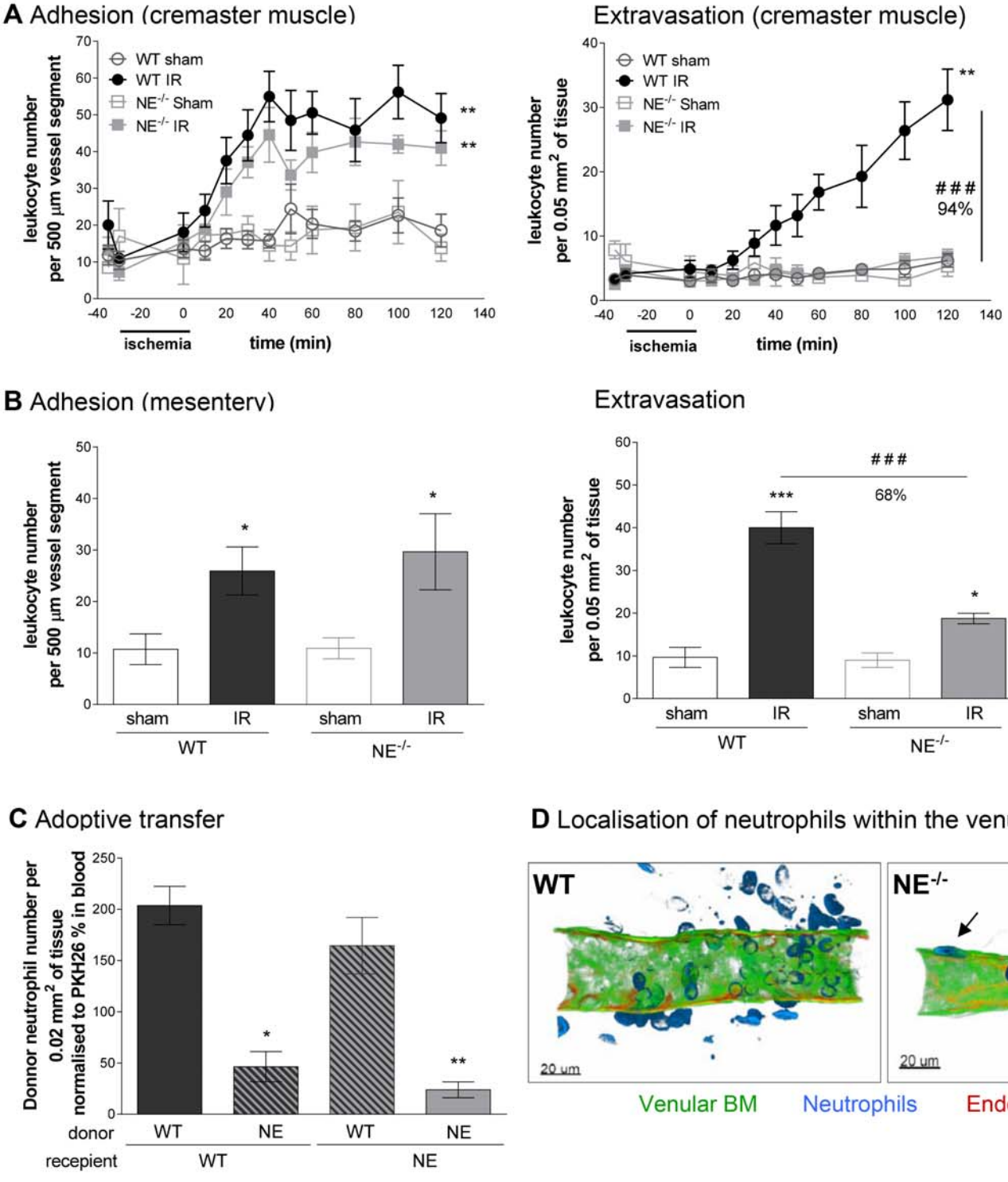
A Adhesion (cremaster muscle)
leukocyte number per 500 µm vessel segment
WT sham
WT IR
NE-/- Sham
NE-/- IR
**
**
ischemia
time (min)
Extravasation (cremaster muscle)
leukocyte number per 0.05 mm2 of tissue
###
94%
B Adhesion (mesentery)
Extravasation
###
68%
***
sham
IR
WT
NE-/-
C Adoptive transfer
Donnor neutrophil number per 0.02 mm2 of tissue normalised to PKH26 % in blood
donor
recepient
D Localisation of neutrophils within the venular BM
WT
NE-/-
20 um
Venular BM
Neutrophils
Endothelial cells
E Cremaster muscle
neutrophil number within venular BM per 200 µm vessel segment
#
I/R
F Mesentery
##

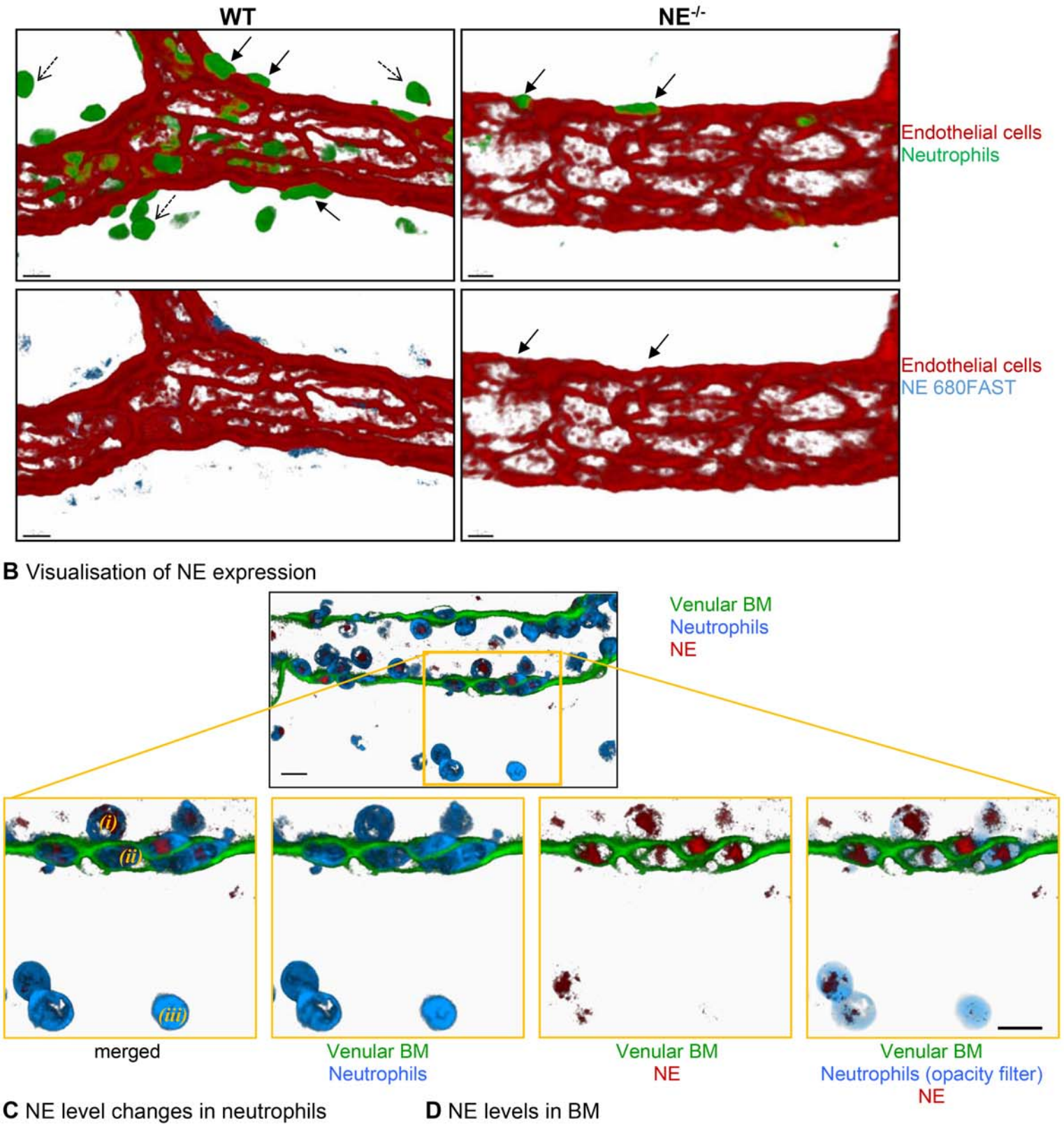
A Visualisation of NE enzymatic activity
WT
NE-/-
Endothelial cells
Neutrophils
Endothelial cells
NE 680FAST
B Visualisation of NE expression
Venular BM
Neutrophils
NE
(i)
(ii)
(iii)
merged
Venular BM
Neutrophils
Venular BM
NE
Venular BM
Neutrophils (opacity filter)
NE
C NE level changes in neutrophils
NE fluorescence insensity in neutrophils (% change)
120
100
80
60
40
20
0
33.6%
*
57.0%
***
lumen (i)
venular BM (ii)
emigrated (iii)
D NE levels in BM
fluorescence intensity (a.u.)
10
8
6
4
2
0
#
**
sham
IR
IR
WT
NE-/-

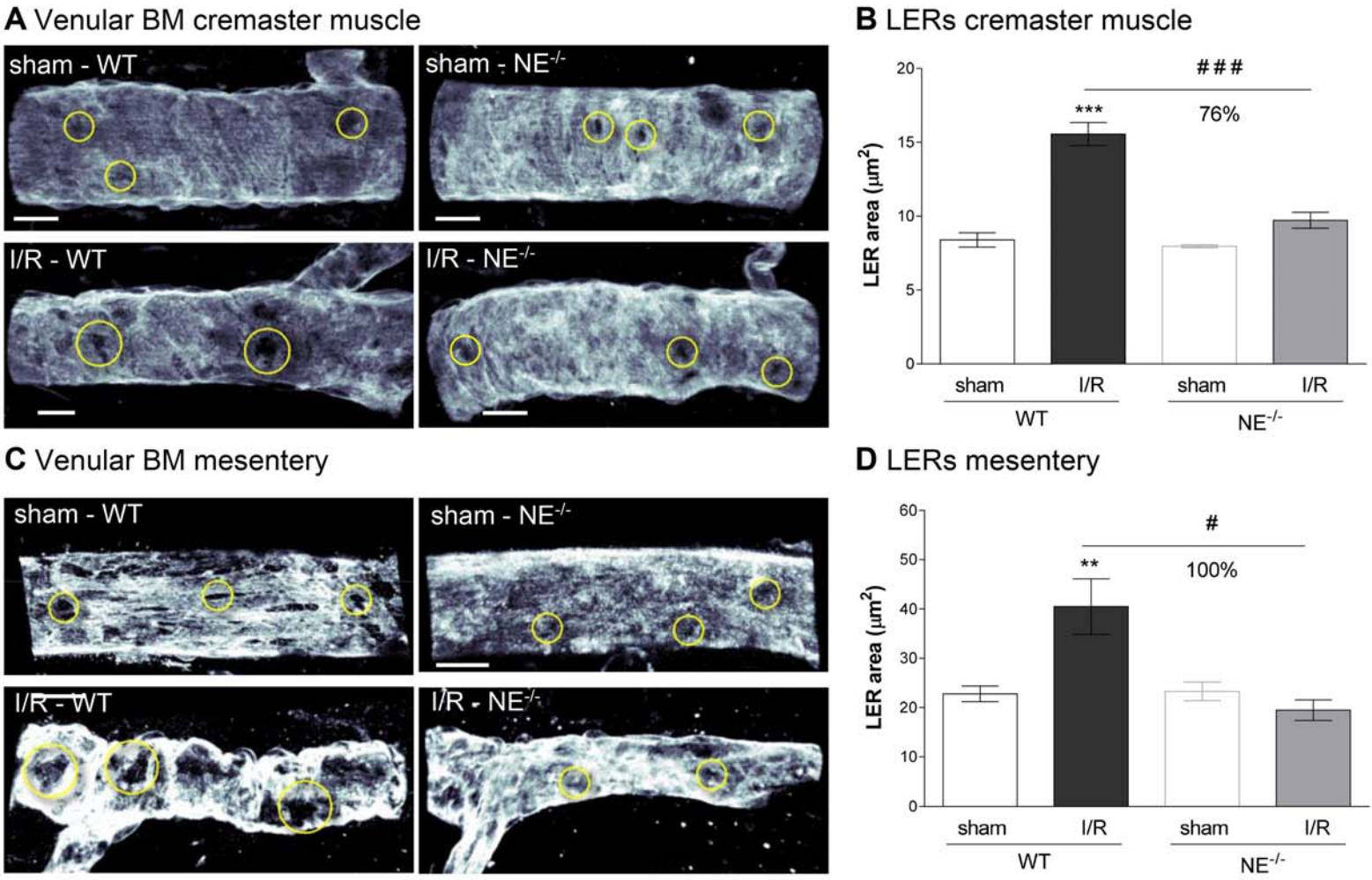
A Venular BM cremaster muscle
sham - WT
sham - NE-/-
I/R - WT
I/R - NE-/-
B LERs cremaster muscle
LER area (μm2)
###
76%
***
sham
I/R
sham
I/R
WT
NE-/-
C Venular BM mesentery
sham - WT
sham - NE-/-
I/R - WT
I/R - NE-/-
D LERs mesentery
LER area (μm2)
#
100%
**
sham
I/R
sham
I/R
WT
NE-/-

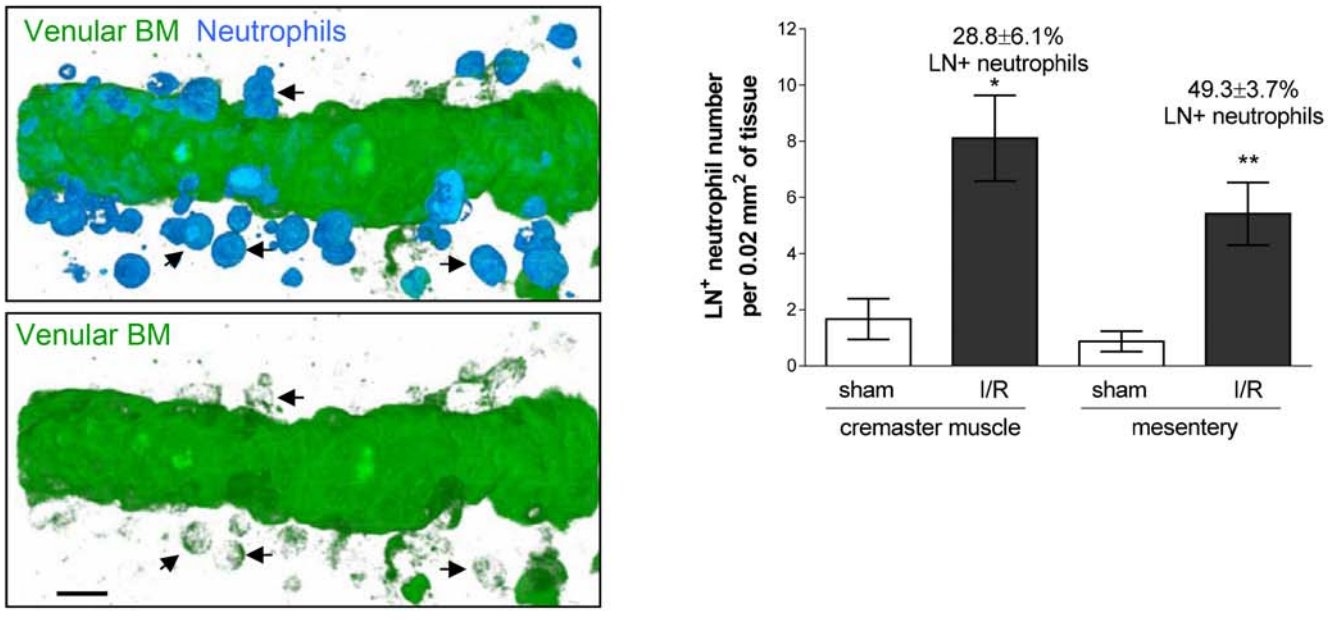
E Venular BM cremaster muscle
Venular BM Neutrophils
Venular BM
F Laminin+ neutrophils
LN+ neutrophil number per 0.02 mm2 of tissue
28.8±6.1%
LN+ neutrophils
*
49.3±3.7%
LN+ neutrophils
**
sham
I/R
sham
I/R
cremaster muscle
mesentery

A Total neutrophils in cremaster muscle (interstitial + vascular)

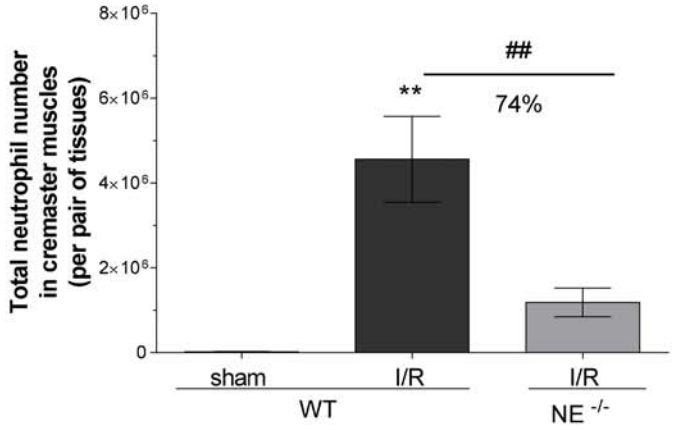

B Neutrophil DHE expression

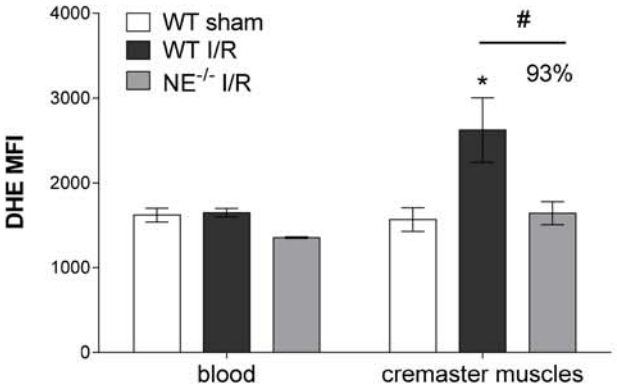

C Vascular leakage in the cremaster muscle

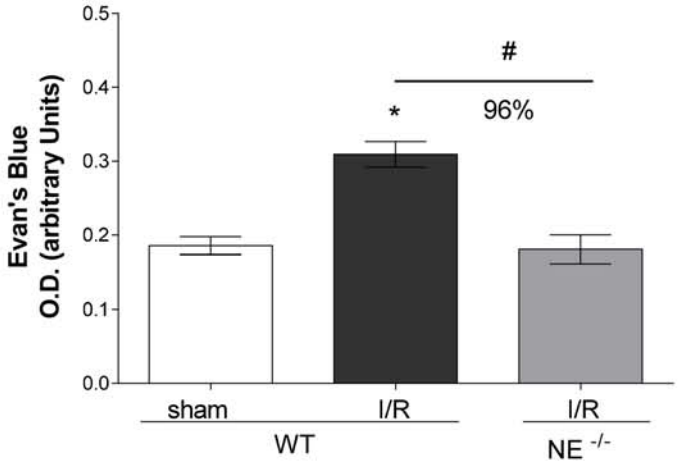

D Total monocytes in cremaster muscles (interstitial + vascular)

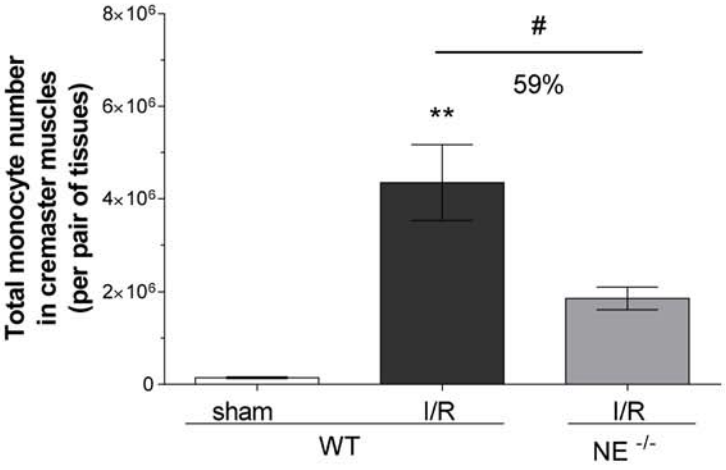

E Total M2 macrophages in cremaster muscles

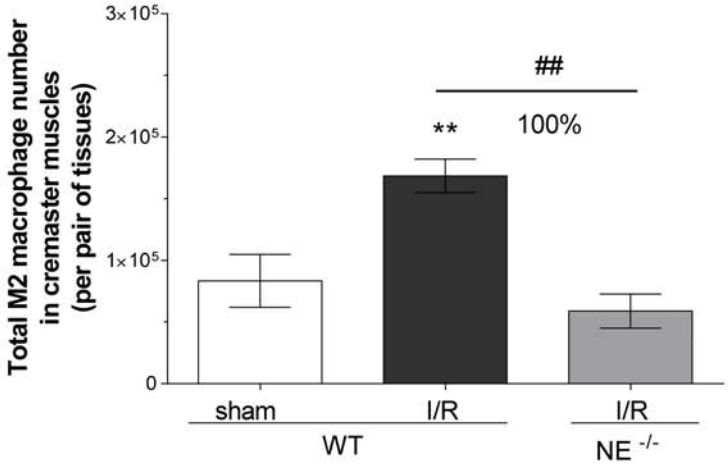

Neutrophil elastase plays a non-redundant role in remodeling the venular basement membrane and supporting neutrophil diapedesis post ischemia/reperfusion injury.

Voisin *et al*. *J Pathol* DOI: 10.1002/path ??? copy ed please add number

Contents:

Supplementary Material and Methods

Reagents/antibodies.

Tyrode's salt, FCS, PFA, EDTA, Triton X-100, collagenase IV, DNase I, rabbit purified IgG, anti-mouse α-SMA antibody (clone 1A4), PKH26 and Evans blue were all purchased from Sigma-Aldrich (Poole, Dorset, UK). Mouse Cytokine and chemokine TNF, IL1β, CXCL1 and CCL2 ELISA kits were from R&D systems (Abingdon, Oxford, UK). Alexa Fluor monoclonal antibody labelling kits and Alexa Fluor fluorescently-labelled secondary antibodies, and CountBright™ Absolute Counting Beads were from Invitrogen (Paisley UK). Anti-mouse antibodies against CD31 (clone 390), CD11b (Mac-1, cloneM1/70) and CD115 (clone AFS98), CD45 (clone 30-F11). Ly6G (clone 1A8), F4/80 (cloneEMR1), CD206 (clone MR6F3) and the isotype controls IgG2b and IgG2a were purchased from eBiosciences (Hatfield, UK) and/or Biolegend (London, UK). Anti-MRP14 [74] (clone 2B10) was a gift from Dr N. Hogg (Cancer Research UK, London, UK). Rabbit anti-mouse NE Ab was generated by Eurogentec (Belgium) and specificity of staining was confirmed in both blood and tissue-infiltrated neutrophils of WT and $NE^{-/-}$ animals (Supplementary material, Figure S4). 123Ecount beads and dihydroethidium (DHE) was purchased from ThermoFisher (Paisley, UK) and NE680FAST was obtained from PerkinElmer (Buckinghamshire, UK).

Animals

Male C57BL/6 wild-type (WT) mice (Harlan, Bicester, UK) and age matched neutrophil elastase knock-out ($NE^{-/-}$) mice were used. $NE^{-/-}$ mice (backcrossed on C57BL/6 background for at least 9 generations) were generated by targeted gene disruption as previously detailed [28] and obtained as a gift from Prof S. Shapiro (Harvard Medical School, Boston, MA, USA). No differences in neutrophil blood counts, vessel diameter or hemodynamics (i.e. wall shear

rate) were noted between WT and $NE^{-/-}$ animals (supplementary material, Figure S2). Animals were housed in individually ventilated cages and facilities were regularly monitored for health status. All animal experiments were conducted in accordance with the United Kingdom Home Office legislations and the number of mice per experimental group was kept to the minimum to reach statistical significance (with a minimal significance level of 0.05% and 80% power) and reproducibility in accordance with NC3R recommendations.

Treatments

Anaesthetized WT mice were injected via jugular vein cannulation with saline or with sivelestat (ONO-5046) (Biotechne, Abingdon, UK) with an initial dose of 50 mg/kg in a 200 µl bolus preceding the induction of ischemia followed by an infusion of 50 mg/kg in 200 µl per hour during the reperfusion period, as per previous works [56].

Ischemia/reperfusion injury of the heart

Anaesthetized animals (150 mg/kg ketamine, 7.5 mg/kg xylazine, i.p.) were subjected to a tracheotomy for artificial ventilation (Harvard Apparatus, AH 40-1000). The tidal volume of the respirator was set at 1 ml/min, with the rate set at 100 strokes/min, and was supplemented with 100% oxygen. After completion of the surgical procedures, mice were allowed to stabilize for 30 min before the ligation of the left anterior descending coronary artery (LADCA) was performed using a 6/0 silk suture (Ethicon, W593 7/0 BV1, Edinburgh, UK). Sham-operated animals received the same surgical procedure without completing the full ligation of the LADCA. Ischemia was confirmed by the appearance of hypokinesis and pallor distal to the occlusion. After a 25 min period of myocardial ischemia, the clip was removed to allow tissue-reperfusion (visually confirmed) for 2 h. At the end of the experiment, mice were killed; heart

removed and ‘snap’ frozen with liquid nitrogen before being processed for cryosectioning and confocal microscopy analysis.

Ischemia/reperfusion injury of the kidneys

Mice were anaesthetized for the duration of surgical procedures (Ketamine 125 mg/kg, i.p.). Animals were subjected to bilateral renal ischemia for 30 min following abdominal laparotomy, during which the renal arteries and veins were occluded using micro-aneurysm clamps as previously described [75]. After the removal of renal clamps the incision was sutured and mice were allowed to recover from anesthesia for 24 h with analgesia (buprenorphine 10 mg/kg s.c.). Sham-operated mice underwent identical surgical procedures without the use of micro-aneurysm clamps. At the end of the experiments, mice were humanly sacrificed, blood samples were taken for serum analysis and kidneys were collected for histological section analysis.

Intravital microscopy and induction of cremasteric ischemia/reperfusion injury

Intravital microscopy (IVM) was used to directly observe leukocyte responses within mouse cremaster venules as previously detailed [32]. In brief, mice were anaesthetized (125 mg/kg Ketamine, 12.5 mg/kg, Xylazine, i.p). The cremaster muscle was surgically exteriorized onto a purpose-built microscope stage and was kept warm and moist by continuous application of warmed Tyrode’s balanced salt solution. Tissue ischaemia was induced by placing an artery clamp at the proximal end of the pinned cremaster tissue for 30 min. Reperfusion was initiated by releasing the clamp and restoring blood flow for up to 2 h. Leukocyte responses were observed on an upright bright-field microscope (Carl Zeiss, Welwyn Garden City, UK). Firmly adherent cells were those remaining stationary for 30 s or longer within a given 500 µm

segment of the endothelial surface of the lumen of postcapillary venules (20–40 µm in diameter). Extravasated leukocytes were quantified within 50 µm on either side of the 500 µm vessel segment in the perivenular tissue. Red blood cell center-line velocity was measured in postcapillary venules with an optical Doppler velocimeter (Microcirculation Research Institute, Texas A&M University, Dallas, TX, USA) and venular wall shear rate was determined based on the Newtonian definition: wall shear rate = 8000 [(red blood cell velocity/1.6)/venular diameter]. At the end of the experiment, mice were humanly killed, tissue removed and fixed in 4% paraformaldehyde (PFA) or 100% ice cold-methanol for 30 min for immunostaining purposes.

Intravital microscopy and induction of ischemia/reperfusion injury of the mesenteric tissue

Anesthetized mice (150 mg/kg Ketamine, 7.5 mg/kg Xylazine, i.p.) were placed in supine position on a heating pad (37 ºC) for maintenance of body temperature. Mesenteric ischemia was induced with a micro-aneurysm clip (Harvard Apparatus), clamping the superior mesenteric artery for 35 min. The clip was then removed, and reperfusion allowed for 90 min. Sham-operated animals underwent the same surgical procedure except for the clamping of the superior mesenteric artery. The mesenteric vascular bed was exteriorized, placed on a purpose-built stage of an upright brightfield microscope (Zeiss Axioskop “FS”). Mesenteries were superfused with warmed (37 ºC) bicarbonate-buffer solution. A 5-min equilibration period preceded the ischemia. Analysis of leukocyte-endothelium interactions was made in 1 to 3 randomly selected post-capillary venules (20–40 µm in diameter, 100 µm in length) for each mouse 90 min post-reperfusion. Leukocyte adhesion (stationary position of the cell for 30 s or longer) was quantified along a 100 µm vessel length. Leukocyte extravasation response was quantified were quantified within 50 µm on either side of the 100 µm vessel segment in the peri-venular tissue. Red blood cell center-line velocity was measured in post-

capillary venules with an optical Doppler velocimeter (Microcirculation Research Institute, Texas A&M University, Dallas, TX, USA) and venular wall shear rate was determined based on the Newtonian definition: wall shear rate = 8000 [(red blood cell velocity/1.6)/venular diameter]. At the end of the reperfusion and analysis period, mice were humanly killed, and mesenteric tissues removed and fixed in 4% paraformaldehyde (PFA) for 30 min prior to immunostaining for observation by confocal fluorescence microscopy.

Determination of renal injury and dysfunction

Blood samples were collected via cardiac puncture for the mouse into S/1.3 tubes containing serum gel (Sarstedt, Germany). The samples were centrifuged (6000 x *g* for 3 min). Serum levels of creatinine and aspartate aminotransferase were quantified by ELISA (R&D systems, Abingdon, Oxford, UK).

Histological evaluation of renal injury

Kidneys were cut in a sagittal section into two halves, fixed in 10% (w/v) PFA at room temperature for 1 week. After dehydration using graded ethanol, tissues were embedded in Paraplast (Sherwood Medical, Mahwah, NJ) and cut into 8 µm-thick sections mounted on glass slides. Sections were then deparaffinized with xylene, stained with hematoxylin and eosin, and viewed under a light microscope (Dialux 22, Leitz, Milan, Italy). For the histopathological score, 100 intersections were examined for each kidney and a score from 0 to 3 was given for each tubular profile involving an intersection: 0, normal histology; 1, tubular cell swelling, brush border loss, nuclear condensation, with up to one third of the tubular profile showing nuclear loss; 2, as for score 1, but greater than one third and less than two thirds of tubular profile show nuclear loss; 3, more than two thirds of tubular profile shows

nuclear loss. The total score for each kidney was calculated by addition of all 100 scores with a maximum score of 300. All the histological studies were performed in a blinded fashion [76]. The total number of infiltrating leukocytes (e.g., neutrophils and mononuclear cells) in cortical interstitial spaces was assessed quantitatively by counting the number of PMNs in high-power fields using x20 or x40 objectives based on the morphology of the nuclei of hematoxylin-eosin stained sections (supplementary material, Figure S1A).

Adoptive cell transfer experiments

To investigate the behavior specifically of WT or $NE^{-/-}$ neutrophils during their migration through the venular wall, adoptive transfer experiments were performed. For this purpose, bone marrow leukocytes from WT or $NE^{-/-}$ donor mice were harvested from the femur and tibia. Cells were then sieved and counted, re-suspended in PBS and incubated with the membrane labelling fluorescent indicator PKH26 according to the manufacturer's recommendations (Sigma) at 37 °C for 30 min. Cells were then injected intravenously into WT or $NE^{-/-}$ recipient animals via the tail vein (10^7 cells/mouse) prior to be subjected I/R injury of the cremaster muscles as detailed above. At the end of the reperfusion period, the cremaster muscles were exteriorized, fixed and immunostained as detailed below for observation by confocal fluorescent microscopy. Blood samples were also taken from cardiac puncture and the number of circulating PKH26+ cells was analyzed by flow cytometry. The results are shown as the number of transmigrated PKH26 cells in 0.02 mm^2 of tissue area per % of PHK26+ cells in the blood in order to normalize the results for the number of blood recirculating cells following the adoptive transfer.

Analysis of tissues by immunofluorescence labeling and confocal microscopy

Detection of neutrophils in the ischemic region of the heart was performed on OCT-embedded heart tissue sections. In brief , sections (30 µm thick) were fixed for 10 min with methanol, permeabilized and blocked in PBS supplemented with 10% FCS, 10% GS and 0.5% Triton X-100 for 1 h and then incubated in PBS + 10% FCS overnight at room temperature with a rabbit anti–mouse collagen IV polyclonal Ab, and fluorescently-labeled rat anti-mouse CD31 and a rat anti–mouse MRP-14 Ab at a concentration of 10 µg/ml to label the endothelium and neutrophils, respectively. Sections were then washed in PBS and incubated with Alexa Fluor-488 labelled goat anti-rabbit for 2 h at RT. Tissue sections were then visualized using confocal microscopy (Zeiss LSM5 Pascal) using 10x (NA:0.25) or 20x (NA:0.50) objectives. Images were subsequently analyzed with IMARIS analysis software (Bitplane, Switzerland). To reconstruct the entire heart sections, serial images were taken and reassembled using Photoshop CS3. Fluorescence intensity quantification was done using IMARIS software using the same settings for all groups.

Detection of neutrophils into the cremaster muscles and mesenteric tissue following I/R injury was performed by immunostaining of whole-mount tissues and visualized by confocal microscopy. In brief, PFA-fixed and permeabilized tissues (PBS containing 10% normal goat serum, 10% of FCS, 5% of mouse serum and 0.5% Triton X-100 for 2 h at room temperature) were immunostained for neutrophils (rat anti-mouse MRP-14 mAb) and the perivascular basement membrane (rabbit anti-mouse LNα-5 mAb, gift from Prof Tanaka) in PBS + 10% FCS overnight at 4 °C. MRP-14 is an intracellular protein highly abundant in neutrophils that is well accepted as a neutrophil specific marker for whole-mount tissues immunostaining and confocal microscopy [74, 77]. Following three washes in PBS, tissues were subsequently incubated with specific Alexa Fluor-633-conjugated anti-rat or Alexa Fluor 555-conjugated anti-rabbit secondary antibodies (Invitrogen) for 4 h at RT in PBS + 10% FCS. In order to stain for endothelial cells, tissues were blocked with rat IgGs for 2 h before adding a rat anti-

mouse Alexa Fluor-488-conjugated CD31 mAb. For NE expression, WT and $NE^{-/-}$ tissues were first immunostained against neutrophils (rat anti-mouse MRP-14) and rabbit anti-NE Abs in PBS + 10% FCS overnight at 4 °C. Following three washes in PBS, tissues were subsequently incubated with specific Alexa Fluor-647-conjugated anti-rat- and -555-conjugated anti-rabbit secondary antibodies for 4 h at RT in PBS + 10% FCS. In order to stain for venular basement membrane, tissues were blocked with rabbit IgGs for 2 h before being incubated with the rabbit anti-mouse Pan-Laminin Ab directly labeled with Alexa Fluor-488 according to the antibody labeling Zenon kit protocol. All samples were viewed using a Zeiss LSM 5 Pascal laser-scanning confocal microscope (Carl Zeiss Ltd, Welwyn Garden City, UK) with a 40× objective (NA:0.75)., All image acquisition parameters for NE expression as quantified by immunostaining and confocal microscopy (e.g. laser power, detector gain voltage, and image format) were normalized to $NE^{-/-}$ tissues. In some experiments, the specificity of staining was also confirmed in WT tissues immunostained with an irrelevant rabbit Ig control antibody (not shown). Acquired Z-stack images were used and analyzed for 3D–reconstruction of whole vessels of 200 µm length (4–6 vessels per tissue) with the image processing software IMARIS allowing to accurately visualize the position of leukocytes relative to the endothelium and the perivascular basement membrane. Mean fluorescent intensity quantification of NE fluorescence was quantified using a mask (isosurface) on the MRP14 or Laminin channels using the same settings throughout the analysis. The area and intensity of matrix protein “Low expression regions” (LERs) within the perivascular basement membrane were measured using ImageJ software (NIH & Laboratory for Optical and Computational Instrumentation, University of Wisconsin, USA) as previously detailed [36, 37].

For the visualization of NE enzymatic activity *in vivo*, mice were subjected to nonsurgical ischaemia using an orthodontic band placed at the top of the scrotums for 35 min followed by 1 h of reperfusion. The NE-fluorescent activatable substrate NE680FAST was injected i.v.

(4.8 nmol per mouse) and a non-blocking Alexa Fluor 555-conjugated rat anti-mouse CD31 (2 µg/mouse) was injected intrascrotally at the end of the ischemic period. At the end of the reperfusion, tissues were harvested, fixed and immunostained with Alexa Fluor 488-conjugated anti-MRP14 Ab as described above. All samples were then viewed using a Leica SP8 laser-scanning confocal microscope with a 20× objective (NA:1) and images of post-capillary venules (at least 6 vessels per tissue) were acquired with the use of sequential scanning of different channels at every 0.5 µm of tissue depth at a resolution of 1024 × 470 pixels in the x × y plane, respectively. This pixel resolution correspond to a voxel size of 0.24 × 0.24 × 0.5 µm in x × y × z. All Images were subsequently analyzed off-line with the 3D-reconstructing image processing software IMARIS (Bitplane, Switzerland).

The specificity of the anti-NE Ab staining was also assessed in blood neutrophils by intracellular immunostaining. In brief, blood leukocytes from WT and $NE^{-/-}$ animals were harvested by cardiac puncture, the erythrocytes lysed with ACK buffer solution (150 mM NH_4Cl, 1 mM $KHCO_3$, 0.1 mM EDTA) and the leukocytes from both genotypes were fixed and permeabilized using BD Cytofix/Cytoperm™ kit according to the reagent protocol. Cells were then incubated with the solution of staining buffer containing 1% of CD16/CD32 blocking reagent and the purified rabbit anti-mouse NE Ab overnight at 4°C. WT or $NE^{-/-}$ cells were also incubated with an Alexa Fluor 555-conjugated or Alexa Fluor 647 rat anti-mouse MRP14, respectively. Cell were then washed four times prior to incubation with an Alexa Fluor 488-conjugated goat anti-rabbit secondary antibody for 2 h at 4 °C. After 4 final washes, both WT and $NE^{-/-}$ samples were then mounted on the same slides with DAPI-containing mounting medium prior to visualization using a Zeiss 800 laser-scanning confocal microscope (Carl Zeiss Ltd, Welwyn Garden City, UK) with a 63× objective (NA:1.4). All Images were subsequently analyzed off-line with the 3D-reconstructing image processing software IMARIS.

Neutrophil and monocyte phenotypic analysis by flow cytometry

The cremaster muscles of WT and $NE^{-/-}$ were subjected to 35 min of nonsurgical ischaemia using an orthodontic band followed by 20 h of reperfusion. Blood (200 µl per animal) was collected by cardiac puncture and the cremaster muscles were harvested and digested into single cell suspension with collagenase and DNase I for 30 min at 37 °C. Cells were fluorescently labeled with conjugated antibodies against CD45, Ly6G, CD11b, CD115, CD206, F4/80 Abs (0.2–2 µg/ml, various fluorochromes) and with FC block for at least 30 min at 4 °C. For Reactive oxygen species (ROS) detection, cells where first pre-incubated with 1 µM of DHE for 15 min at 37 °C prior to the incubation with antibodies. CountBright™ Absolute Counting Beads were used to quantify the total number of cells following manufacturer's recommendations. Samples were analyzed using a BD LSR-Fortessa (BD Biosciences) and FlowJo analysis software (Treestar, BD Biosciences). Leukocytes were first gated with CD45 and FCS/SSC morphology (excluding cell doublet). Neutrophils were identified as CD45+ CD11b+ Ly6G+, monocytes were identified as CD45+ Ly6G- CD11b+, CD115+, $F4/80^{low}$; and M2 macrophage were identified as CD45+ Ly6G- $CD11b^{high}$, F4/80+, CD206+.

Vascular leakage assay (Evan's blue Miles Assay)

Vascular leakage was assessed in the mouse cremaster muscle of WT and $NE^{-/-}$ mice following ischemia/reperfusion injury. In brief, cremaster muscles were subjected to 35 min of nonsurgical ischaemia using an orthodontic band followed by 2 h of reperfusion. Mice where then injected intravenously with 0.5% Evans Blue solution (6 µl/g body weight). Two hours later (i.e. 4 h post reperfusion), mice were sacrificed and the cremaster muscles were excised and incubated in 100% formamide overnight at 56 °C. The optical density of eluted

Evans Blue in 50 µl of samples was measured by spectrophotometry at wavelength of 620 nm. Results are presented as optical density (OD) of Evans Blue leakage [31].

Statistical analyses

All data was processed and analyzed using Prism 4 software (GraphPad Inc, San Diego, CA, USA). Statistical significance was assessed by parametric (one-way/two-way ANOVA followed by Newman-Keuls multiple comparison test) and non-parametric (Kruskal-Wallis followed Dunn's multiple comparisons test) tests according to the sample size of the data analyzed. Where only two variables were analyzed, an unpaired *t*-test (Mann-Whitney) was used. $P < 0.05$ taken as significant. Results are given as mean $\pm$ SEM.

Supplementary Figures

Supplementary Figure S1

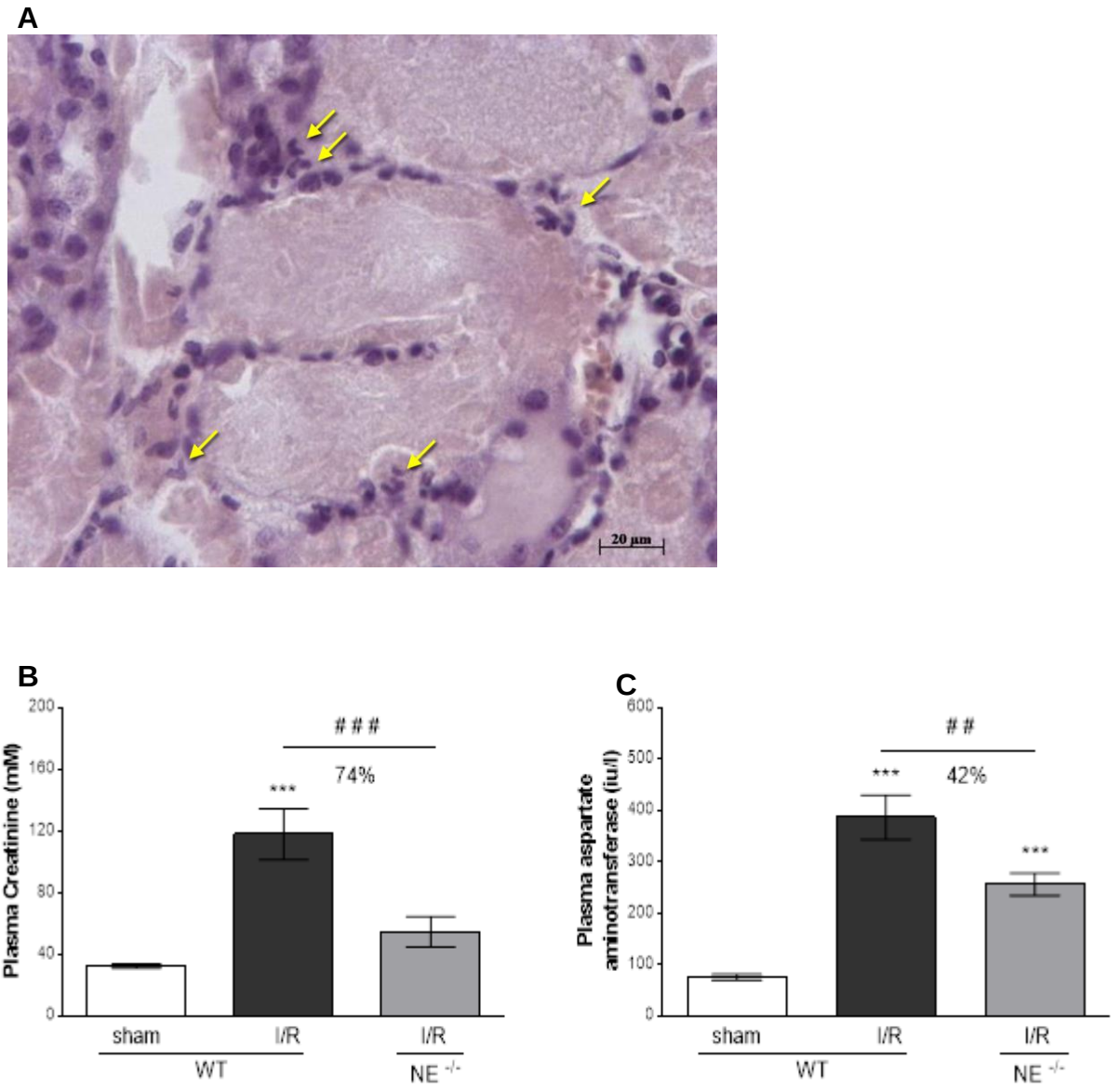

Supplementary Figure S1. Assessment of renal dysfunction following kidney ischemia/reperfusion injury (I/R injury). WT and $NE^{-/-}$ mice were subjected to bilateral renal ischemia for 30 min followed by a 24 h reperfusion period. (**A**) H&E staining of kidney sections showing the presence of PMNs (yellow arrows) in the interstitium of the kidney of a WT mice subjected to I/R injury (x40 objective magnification). Bar = 20 µm. The levels of creatinine (**B**)

and aspartate aminotransferase (**C**) in mouse plasma were measured as biochemical markers of renal dysfunction subsequent to sham-operation (WT) or renal ischemia/reperfusion injury (WT and $NE^{-/-}$ animals). Data represent mean ± SEM. *** P<0.001 (5 mice per group) for comparison between I/R versus sham operated animals; and ## P<0.01, ### P<0.001 for comparison between WT and $NE^{-/-}$ mice as indicated by lines.

Supplementary Figure S2

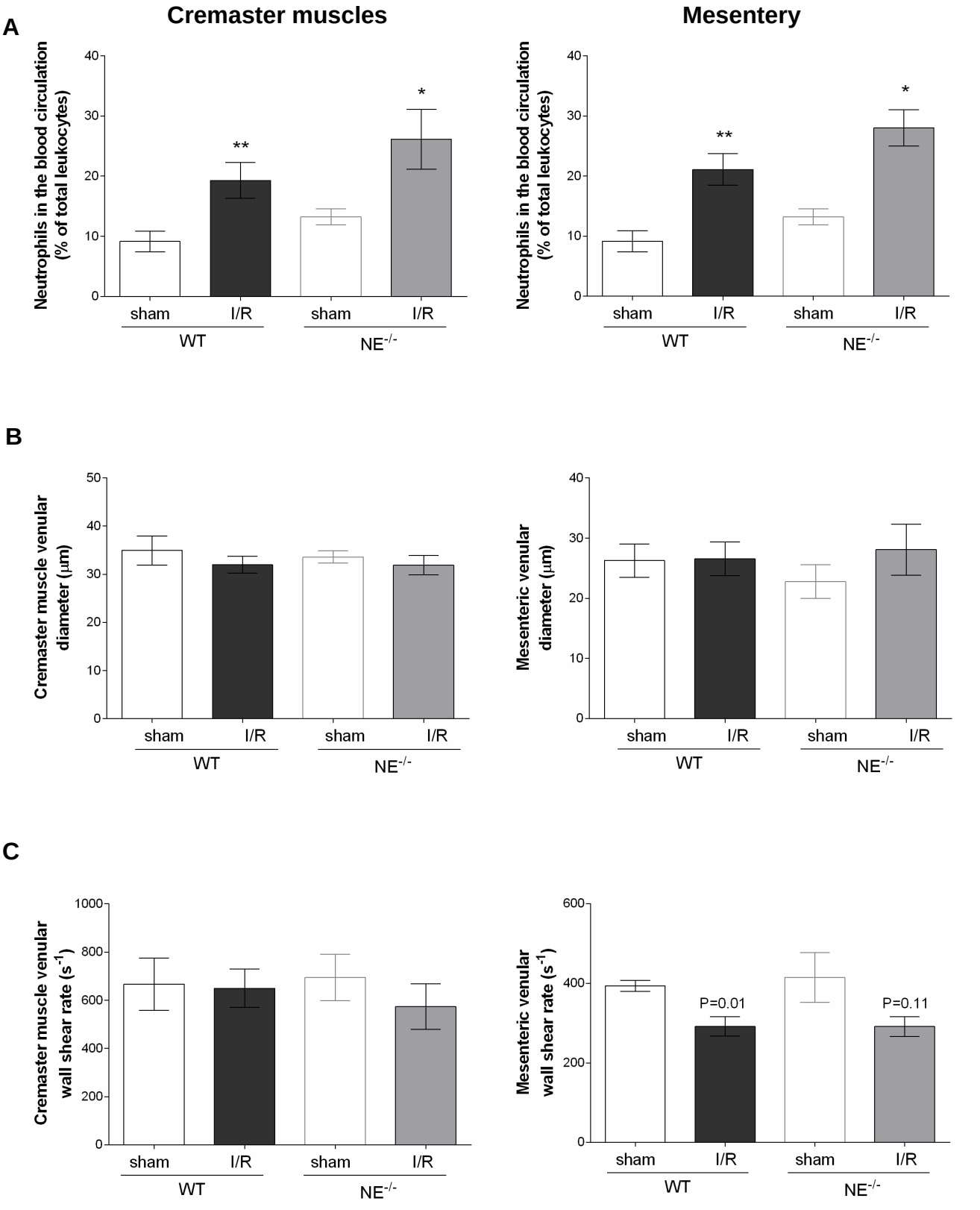

Supplementary Figure S2. Assessment of blood neutrophils, vessel diameter and hemodynamics of postcapillary venules in WT and NE$^{-/-}$ animals. The cremaster muscles or mesentery of WT and NE$^{-/-}$ Mice were subjected to ischemia/reperfusion (I/R) injury (30 min/2 h for the cremaster muscles or 35 min/90 min for the mesentery) for analysis of leukocyte responses by bright-field intravital microscopy and flow cytometry. (**A**) Percentage of circulating neutrophils (of total leukocyte counts) in the blood of animals subjected to I/R of the cremaster muscles (left panel) or mesentery (right panel) and as analyzed by flow cytometry. (**B**) Diameters of post-capillary venules of animals subjected to I/R of the cremaster muscles (left panel) or mesentery (right panel) as measured by bright-field intravital microscopy (**C**) Wall shear rate within post-capillary venules of animals subjected to I/R of the cremaster muscles (left panel) or mesentery (right panel) as measured by bright-field intravital microscopy. Data represent means ± SEM per mouse. * $P<0.05$, ** $P<0.01$ (at least 5 mice per group) for comparison between I/R versus sham operated animals.

Supplementary Figure S3

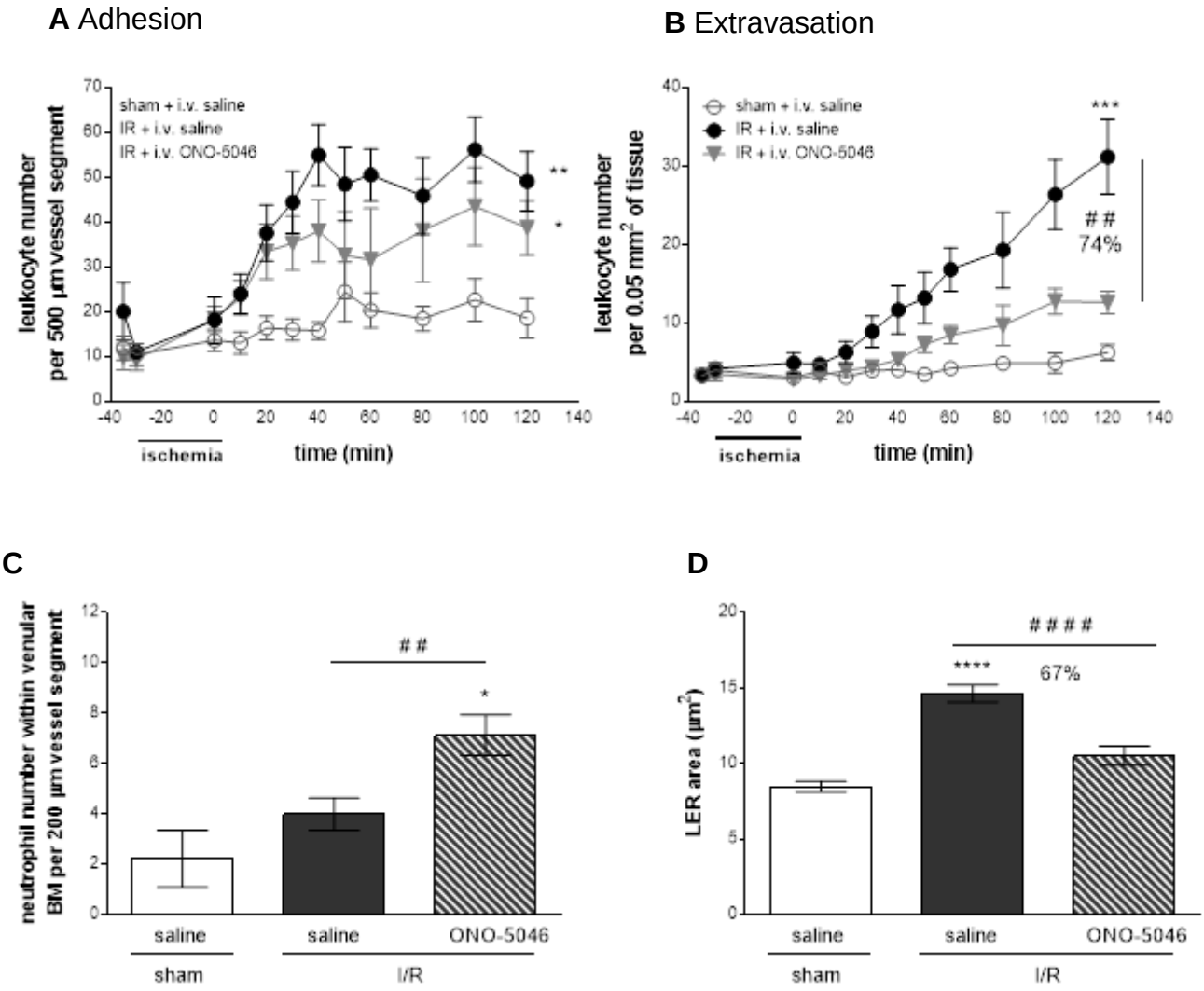

Supplementary Figure S3. Pharmacological inhibition of neutrophil elastase blocks the migration of neutrophils at the level of the basement membrane post I/R injury. Leukocyte migration responses in the cremaster muscle of WT mice subjected to I/R injury were investigated by intravital and confocal microscopy. To inhibit NE, mice received an intravenous bolus injection of the NE-specific inhibitor ONO-5046 (sivelestat) followed by a continuous infusion of this inhibitor (50 mg/kg/h) before the induction of ischemia. Control animals received saline. Leukocyte adhesion (**A**) and extravasation (**B**) responses were quantified at regular intervals for 120 min from the start of the reperfusion period. (**C**) At the

end of the experiment, tissues were harvested, fixed and immunostained with fluorescent antibodies against neutrophils (MRP14), endothelial cells (CD31) and the basement membrane (Laminin-α5) prior to the visualization of the vessels by confocal microscopy. The number of neutrophils present within the venular basement membrane was quantified for each group of animals. (**D**) Quantification of the size of the basement membrane low expression regions (LERs) from cremaster postcapillary venules of mice subjected to I/R injury and/or treated with the NE inhibitor ONO-5046. Data are from at least 5 mice per group and are presented as mean ± SEM. * P<0.05, ** P<0.01, *** P<0.001, **** P<0.0001 for comparison between I/R versus sham operated animals; and ## P<0.01, #### P<0.0001 for comparison between ONO-5046 and saline-treated animals as indicated by lines.

Supplementary Figure S4

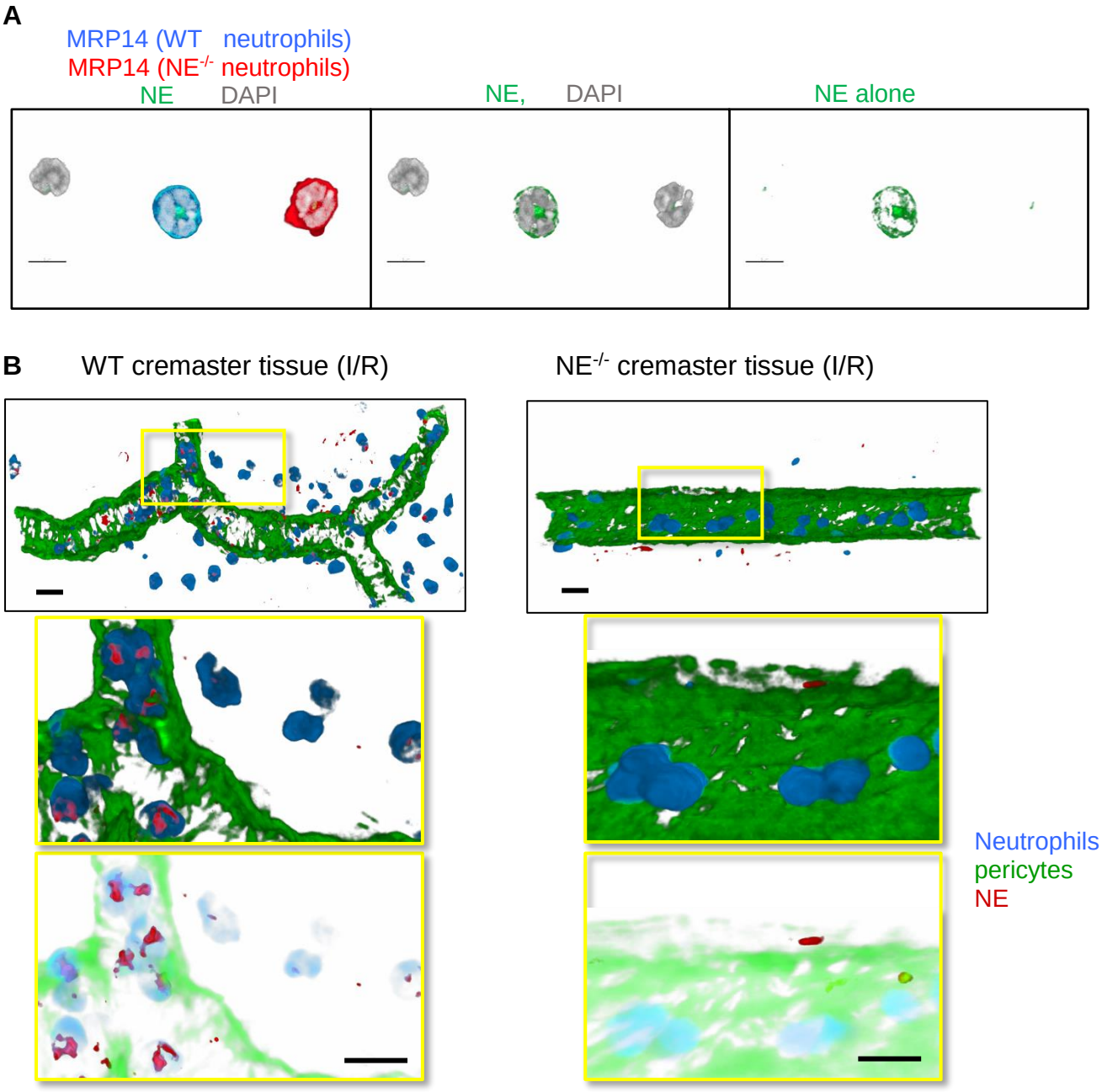

Supplementary Figure S4. Specificity of a new rabbit anti-mouse NE antibody. (**A**) Blood leukocytes from WT and $NE^{-/-}$ animals were immunostained for NE with a rabbit anti-mouse NE antibody (green) and neutrophils and rat anti-mouse MRP14 conjugated with Alexa Fluor 555 (blue) or Alexa Fluor 647 (red) fluorochromes for WT or $NE^{-/-}$ cells, respectively. The nuclei of the leukocytes were revealed with DAPI staining. The images show that WT but not $NE^{-/-}$ neutrophils, exhibit a positive staining for NE in the cytoplasm but

not the nucleus of the cell. (**B**) Cremaster muscles of WT and $NE^{-/-}$ mice subjected to I/R injury were harvested, fixed and immunostained for neutrophils (MRP14, blue), pericytes (α-SMA, green) and neutrophil elastase (red) prior to imaging by confocal microscopy. The images are representative of a WT (left panels) or $NE^{-/-}$ (right panels) mouse post-capillary venule showing the expression of NE by WT, but not $NE^{-/-}$ neutrophils. A 5% opacity filter on the MRP14 and α-SMA channels was applied to better visualize NE expression within neutrophils in the bottom images. Images are representative pictures from n=3 independent experiments. Bar = 10 μm.

Supplementary Figure S5

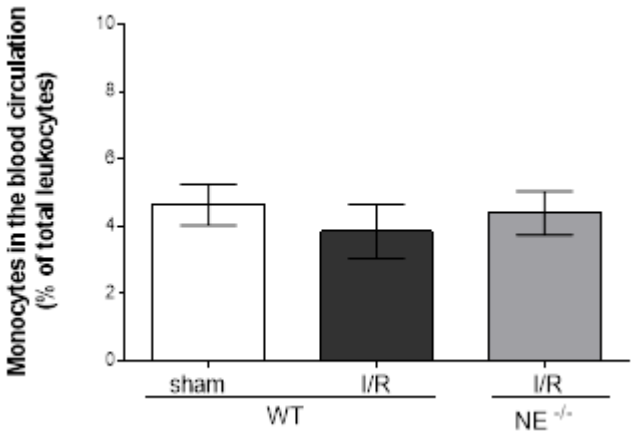

Supplementary Figure S5: Assessment of blood monocytes of WT and NE$^{-/-}$ animals following I/R injury. The cremaster muscles of WT and NE$^{-/-}$ mice were subjected to 30 min of ischemia followed by a 20 h reperfusion period. The graph shows the quantification of the percentage of circulating neutrophils (of total leukocyte counts) in the blood of animals subjected to I/R of the cremaster muscles (left panel) or mesentery (right panel) and as analyzed by flow cytometry.

Supplementary Movie legends

Movie S1. Bright-field intravital microscopy of the NE$^{-/-}$ cremaster muscle subjected to ischemia/reperfusion injury. The movie captures the development of the inflammatory response (leukocyte recruitment) of a post-capillary venule from the cremaster muscle of a WT mouse subjected to ischemia (30 min) and reperfusion (120 min) injury as recorded by bright-field intravital microscopy. Red blood cell velocity was measure with an optical Doppler velocimeter (black dots). Quantification of the inflammatory response is shown in Figure 3A.

Movie S2. Bright-field intravital microscopy of the NE$^{-/-}$ cremaster muscle subjected to ischemia/reperfusion injury. The movie captures the development of the inflammatory response (leukocyte recruitment) of a post-capillary venule from the cremaster muscle of a NE$^{-/-}$ mouse subjected to ischemia (30 min) and reperfusion (120 min) injury as recorded by bright-field intravital microscopy. Red blood cell velocity was measure with an optical Doppler velocimeter (black dots). Quantification of the inflammatory response is shown in Figure 3A.

Movie S3. Bright-field intravital microscopy of the mesenteric tissue subjected to ischemia/reperfusion injury. The movie captures the leukocyte inflammatory response of post-capillary venules from the mesentery of WT and NE$^{-/-}$ mice at 90 min post reperfusion as recorded by bright-field intravital microscopy. Quantification of the inflammatory response is shown in Figure 3B.